DEVELOPMENT OF
AN IMPEDANCE GLOTTOGRAPH

A dissertation submitted in
partial fulfillment of the requirements for the degree of

Master of Technology

by

P. S. Rajath Bhat
(09307R02)

under the supervision of

Prof. P. C. Pandey

Department of Electrical Engineering
Indian Institute of Technology Bombay
June 2012

Indian Institute of Technology Bombay

M. Tech. Dissertation Approval

This dissertation entitled **"Development of an Impedance Glottograph"** by **P. S. Rajath Bhat** (Roll No. **09307R02**) is approved, after the successful completion of *viva voce* examination, for the award of the degree of **Master of Technology** in **Electrical Engineering.**

Supervisor ..... (Prof. P. C. Pandey)

Examiners ..... (Prof. Joseph John)

..... (Prof. L. R. Subramanyan)

Chairperson ..... (Prof. R. C. Prasad)

Date: 28 June 2012

Place: Mumbai

DECLARATION

I declare that this written submission represents my ideas and my own words and where other's ideas or words have been included, I have adequately cited and referenced the original sources. I also declare that I have adhered to all principles of academic honesty and integrity and have not mispresented or fabricated or falsified any idea/data/fact/source in my submission. I understand that any violation of the above will be cause for disciplinary action by the Institute and can also evoke penal action from sources which have thus not been properly cited or from whom proper permission has not been taken when needed.

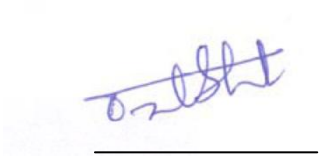

Date: June 2012

Place: Mumbai

(P. S. Rajath Bhat)

P. S. Rajath Bhat / Prof. P. C. Pandey (Supervisor), “Development of an Impedance Glottograph,” *M. Tech. dissertation*, Department of Electrical Engineering, Indian Institute of Technology Bombay, June 2012.

Abstract

Impedance glottography is a noninvasive method to monitor the degree of contact between the vibrating vocal folds. Time-varying electrical impedance, measured by placing a pair of electrodes on either side of the thyroid cartilage, is used for diagnosing voice disorders, estimation of pitch, and speech training aids. The objective of the project is to develop (a) a laryngeal impedance simulator for testing the sensitivity and frequency response of the impedance glottograph instrument, and (b) an impedance glottograph instrument using novel circuits for improving the frequency response and noise rejection.

A laryngeal impedance simulator, using a microcontroller, analog switches, and digital potentiometer is developed and tested. Simulation parameters (frequency, basal resistance and change in basal resistance) are set through serial port. An impedance glottograph instrument, consisting of a sinusoidal source, voltage-to-current converter, voltage sense amplifier, and synchronous demodulator, has been designed and tested. A voltage, in the frequency range of 50–500 kHz, generated using a direct digital synthesizer (DDS) is given as input to a voltage-to-current converter with complementary current outputs, designed using a pair of transconductance amplifiers to output a low amplitude (< 5 mA) current. This current is injected using a pair of electrodes held in contact with the skin on both sides of the thyroid cartilage. The resulting amplitude modulated voltage is amplified using a voltage sense amplifier and given to the demodulator. Synchronous demodulation with current steering and baseline restoration circuit is used to get the demodulated waveform, representing the impedance variation. Sampling of the demodulator waveform in synchronism with the peaks of the excitation waveform is used for improving ripple rejection.

Contents

List of Figures and Tables

List of Abbreviations

Abbreviation	Term
DDS	direct digital synthesizer
EGG	electroglottography
EMGG	electromagnetic glottography
FGG	flow glottogram
IGG	impedance glottography
L_X	laryngogram
OTA	operational trans-conductance amplifier
SPI	serial peripheral interface

Chapter 1

INTRODUCTION

1.1 Overview

Organs involved in speech production can be divided in three main groups: lungs, larynx, and the vocal tract. Lungs are the source of airflow which passes through the larynx and the vocal tract, finally exiting from the mouth. Larynx has two muscular membranes stretched horizontally, called vocal folds. The space between the folds is known as the glottis. Air expelled from lungs through the glottis creates pressure difference across the vocal folds, causing vibration, resulting in an air flow. This process is known as phonation. Vocal tract, which acts as a time-varying acoustic filter, consists of laryngeal cavity, pharynx, oral cavity, and nasal cavity. Sound waves, generated due to phonation, pass through the vocal tract resulting in articulation or speech production [1], [2].

Laryngeal diseases affect the phonation mechanism causing abnormal speech. Monitoring of the movement of the vocal folds is important for diagnosing laryngeal diseases. Location of the vocal folds causes difficulties in analysis of their functioning, because a direct measurement of their movement is difficult. The techniques used for monitoring vocal folds can be broadly classified into visual, acoustic, and indirect methods [4]. Table 1.1 summarizes different methods and associated techniques.

The visual methods of measuring vocal tract movement, described briefly in Appendix A, are invasive and uncomfortable. Visual and acoustic methods give information about separation of the vocal folds but very little information about nature of the vocal folds contact. Impedance glottography or electroglottography, a non-invasive method, is used to measure the vocal fold contact during voicing without affecting speech production [3]. It gives information about the contact phase of the vocal folds [13]. It is based on sensing of electrical impedance. It was first reported by

Table 1.1 Techniques for monitoring vocal folds

Method	Techniques
Visual	Laryngoscopy [3], [4], videokymography [5], stroboscopic imaging[6], high speed photography[7], and photoglottography [8]
Acoustic	Inverse filtering[9]
Indirect	Ultrasonoglottography[10] and electroglottography [11],[12]

Fabre (1957), and other significant contributions have been made by Frokjaer-Jensen (1968) and Fourcin (1971) [4]. An electrode pair is placed over the skin on each side of the thyroid cartilage. The impedance between the electrodes increases as contact between the vibrating vocal folds decreases and impedance decreases as contact between the vibrating vocal folds increases. This technique allows recording of contact pattern of vocal folds continuously over time. This is a low cost and easy to use method. However, it does not provide information as the motion of the vocal cords during the open phase [11], [12].

1.2 Project objective

Development work for electroglottograph has been carried out at IIT Bombay as part of several student projects [25]–[31]. The objective of the project is to develop (a) a laryngeal impedance simulator for testing the sensitivity and frequency response of the impedance glottograph instrument and (b) an impedance glottograph instrument using novel circuits for improving frequency response and noise rejection.

1.3 Outline of the dissertation

The second chapter gives an overview of the techniques for the evaluation of laryngeal behavior. It also gives a detailed description of the impedance glottography technique and a review of development work carried out at IIT Bombay. The hardware design of laryngeal impedance simulator has been reported in the third chapter. Chapter 4 describes the design and implementation of impedance glottograph. Summary and conclusion are given in the last Chapter. Supplementary information is provided in the appendices.

Chapter 2

IMPEDANCE GLOTTOGRAPHY

2.1 Speech production

Vocal tract refers to the portion above the larynx and includes oral cavity, nasal cavity, tongue, lip and pharynx. Figure 2.1 shows the overview of the vocal tract and parts that are important in speech production. Speech production comprises of two mechanical functions namely phonation and articulation. Phonation takes place in the larynx whereas articulation is carried out in the vocal tract. During normal breathing, the air passes through the larynx and vocal tract remains unobstructed creating no or little sound [1], [2]. The source of most speech occurs in the larynx where the vocal folds partially or completely obstruct the air flow from the lungs. When the air is expired, its pressure pushes the vocal folds apart and air flows rapidly. This rapid flow of air causes Bernoulli effect, causing vocal folds to pull towards each other. This stops the air flow, building pressure again which again opens the vocal folds, causing the vocal folds to vibrate. The rate of vibration is called the fundamental frequency or the pitch. Typical pitch range for male and female speakers are 100–250 Hz and 200–450 Hz, respectively.

2.2 Basics of impedance glottography

The impedance glottography (EGG), electroglottography (EGG), or laryngography is a noninvasive technique to monitor the glottal activity by measuring the variation in electrical impedance between two electrodes placed on both sides of the thyroid cartilage. Electrodes are held in contact with the skin, allowing the speaker to speak and breathe naturally. The vibration of vocal folds is monitored by measuring the variation in electrical impedance across the electrodes. The contact pattern of vocal folds is represented as a time-varying signal known as electroglottogram, or laryngogram (L_x) [2].

Figure 2.2 shows the sequence of vocal folds vibrations [16]. There are three phases: opening phase, separation phase, and contact phase. In opening phase, the air

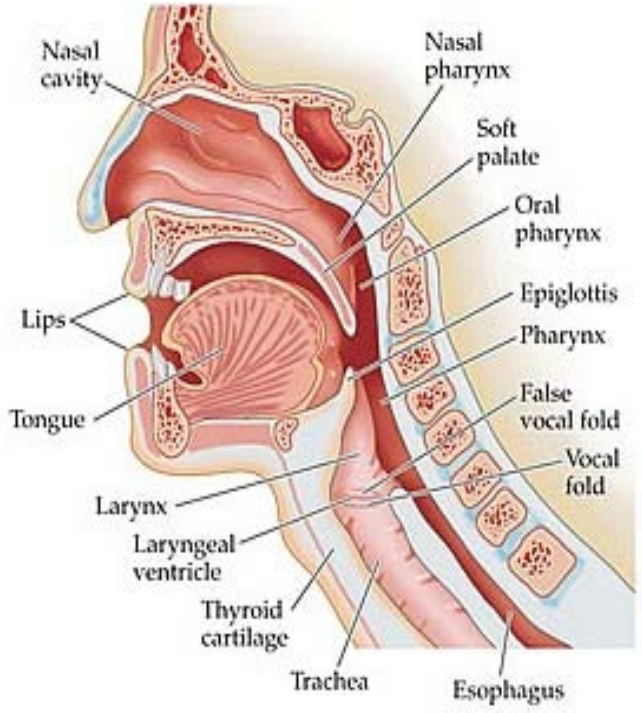

Figure 2.1: Speech production mechanism [14]

between the vocal folds tissues results in high electrical impedance. During separation, the air between the folds decreases but the electrical impedance remains high. During contact phase, the electrical impedance decreases due to contact of the folds. Hence, the impedance increases when folds are in the opening and separation phases and decreases during the closing phase, resulting in EGG waveform, which is inversely related to the vocal folds contact pattern as shown in Figure 2.3 [15].

The impedance glottogram or electroglottogram is generally obtained during the utterance of an isolated vowel such as /i/ by the speaker. EGG is a depiction of vocal fold contact area. It is a waveform whose slope increases during the opening phase and decreases during the closing phase of the contact area of vocal folds [17].

Parameters estimated from electroglottogram are open quotient, close quotient, speed quotient, pitch period, and fundamental frequency [17]. Figure 2.3 shows different glottal phases in the EGG waveform. Opening phase starts when slope of the curve begins to increase (vocal folds opening) and ends at the highest peak (folds completely open). Contact phase starts when slope of curve begins to decrease (folds closing) and ends at the lowest point (folds completely closed).

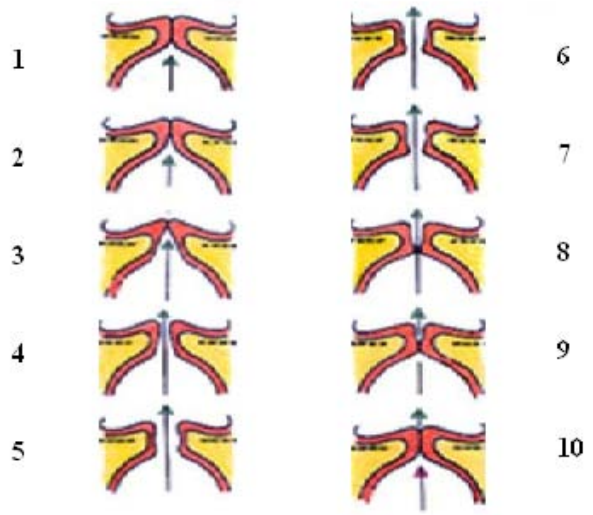

Figure 2.2: Vocal folds vibration sequence. Opening phase (1-3), complete separation (4-7), closing phase (8-10) [16].

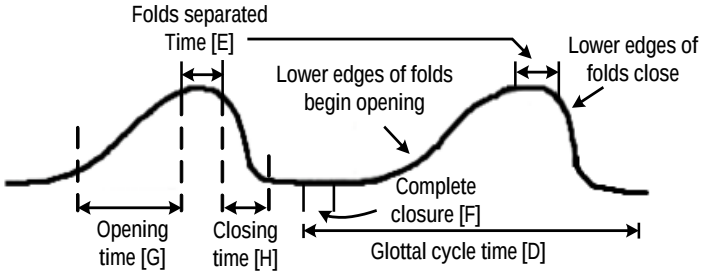

Figure 2.3: EGG waveform [4]

Speed quotient (SQ) is defined as the ratio of the duration of the opening phase T_G to the duration of the contact phase T_H.

$$SQ = T_G / T_H \tag{2.1}$$

Open quotient (OQ) is defined as the ratio of the separation duration T_E to the glottal period T_D. Separation duration is the time when the folds are separated.

$$OQ = T_E / T_D \tag{2.2}$$

Close quotient (CQ) is defined as the ratio of the duration of the complete closure of the folds T_F to the glottal period T_D.

$$CQ = T_F / T_D \tag{2.3}$$

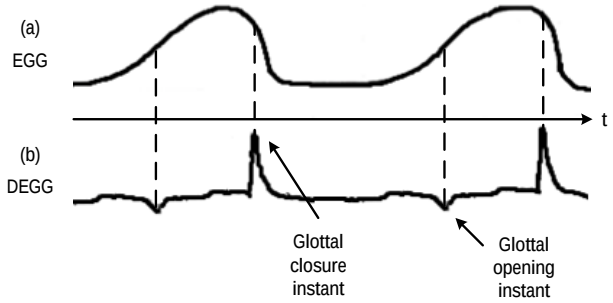

Figure 2.4: (a) EGG signal (b) DEGG [18]

The differential of the EGG, as shown in Figure 2.4, is known as DEGG. The rate at which vocal folds vibrate is known as the fundamental frequency. It is the reciprocal of the pitch period which can be measured as the period between two peaks of DEGG [18].

There are several application of the EGG waveform in the assessment of vocal disorders and speech analysis.

(a) *Pathology:* The EGG signal gives the variation of impedance due to movement of vocal folds, which depends on the pathological condition of vocal folds. Analysis of EGG waveform, such as the closing rate and closed percentage, are particularly useful in assessing the degree of vocal fold tension, muscle stiffness or weakness [18].

(b) *Estimation of fundamental frequency:* Fundamental frequency or pitch can be calculated easily from EGG with high accuracy. The differential of EGG can be used to calculate pitch value by finding the time period between either zero crossings or between minima of differential EGG waveform [18].

(c) *Voicing detection:* Thresholding of EGG is used to classify voiced and unvoiced signal. For voiced speech, EGG is periodic and large in amplitude. For unvoiced signal, EGG is almost zero [19].

Some of the commercially available instruments are

(a) Laryngograph microProcessor, marketed by Laryngograph Limited of UK [20].

(b) VoceVista, marketed by Vocevista of Netherlands [21].

(c) lingWAVES EGG, marketed by WEVOSYS of Germany [22].

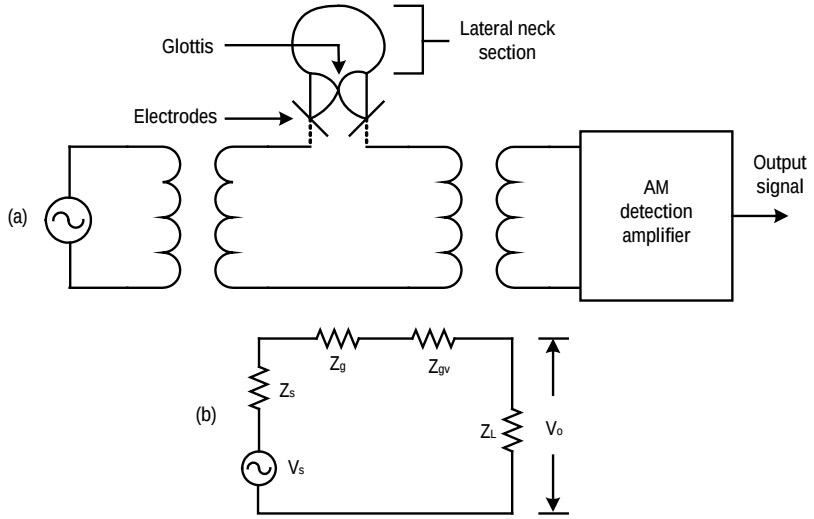

Figure 2.5: (a) Impedance detection method described by Childers and Larar [19]
(b) Equivalent circuit

(d) EG 90, marketed by F-J Electronics of Denmark [23].

(e) EG2-PCX2, by Glottal Enterprise, marketed by Tiger DRS, Inc. [24].

2.3 Impedance detection methods

Several methods have been used to detect the glottal impedance variation. The impedance detection scheme of Childers and Larar [19] is shown in Figure 2.5 (a). A pair of electrodes is placed on both sides of the thyroid cartilage. A high frequency voltage signal is applied using a transformer and the resulting amplitude modulated voltage is picked up by using another transformer. Equivalent circuit of the scheme is given in Figure 2.5 (b). The impedance between the electrodes can be modeled as fixed impedance Z_g varying impedance Z_{gv}. Z_s is the source impedance and Z_L is the input impedance of the detecting circuit. Thus,

$$V_o = V_S \frac{Z_L}{Z_L + Z_S + Z_g + Z_{gv}}$$

$$\approx V_S \left[\frac{Z_L}{Z_L + Z_S + Z_g} \right] \left[1 - \frac{Z_{gv}}{Z_L + Z_S + Z_g} \right] \qquad (2.4)$$

When the vocal folds vibrate, Z_{gv} changes, resulting in amplitude modulated output. Resultant modulation index is small as Z_{gv} is small as compared to (Z_L+ Z_s + Z_g).

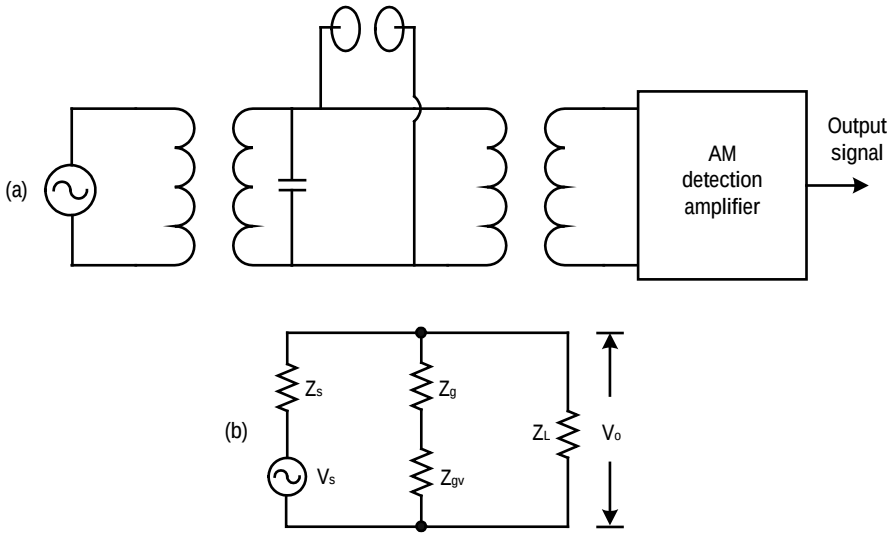

Figure 2.6: (a) Impedance detection method used in instrument patented by Rothenberg [39] (b) Equivalent circuit

The impedance detection scheme used by Rothenberg [35] is shown in Figure 2.6 (a). A high frequency voltage signal is applied across the electrodes which are in parallel with the source and sensing transformers. An equivalent model can be given as shown in Figure 2.6 (b). The impedance between the electrodes can be modeled as fixed impedance Z_g in series with time-varying impedance $Z_{gv,}$ Z_s is source impedance and Z_L is the input impedance of the AM detection amplifier, Thus,

$$V_O = V_S \frac{Z_L \| \left(Z_g + Z_{gv} \right)}{Z_S + Z_L \| \left(Z_g + Z_{gv} \right)}$$

$$\approx V_S \left[\frac{Z_L}{Z_L + Z_S + Z_L Z_S / Z_g + Z_g \left(Z_S + Z_L \right) / Z_g} \right] \left[1 + \frac{Z_{gv}}{Z_g} \right] \qquad (2.5)$$

When the vocal folds vibrate, Z_{gv} changes resulting in amplitude modulated output.

The impedance detection scheme used by Fourcin [36] is shown in Figure 2.7 (a). A pair of central disc and ring electrode is held over the skin on both sides of thyroid cartilage. A transformer is used to apply high frequency voltage signal across the central disc and ring on one side. The output voltage between its central disc and ring on the other side is sensed. The source side electrode is referred to as the transmitter and the sensor side electrode is referred to as the receiver. An equivalent circuit of scheme is given in Figure 2.7(b). The impedance between the electrodes

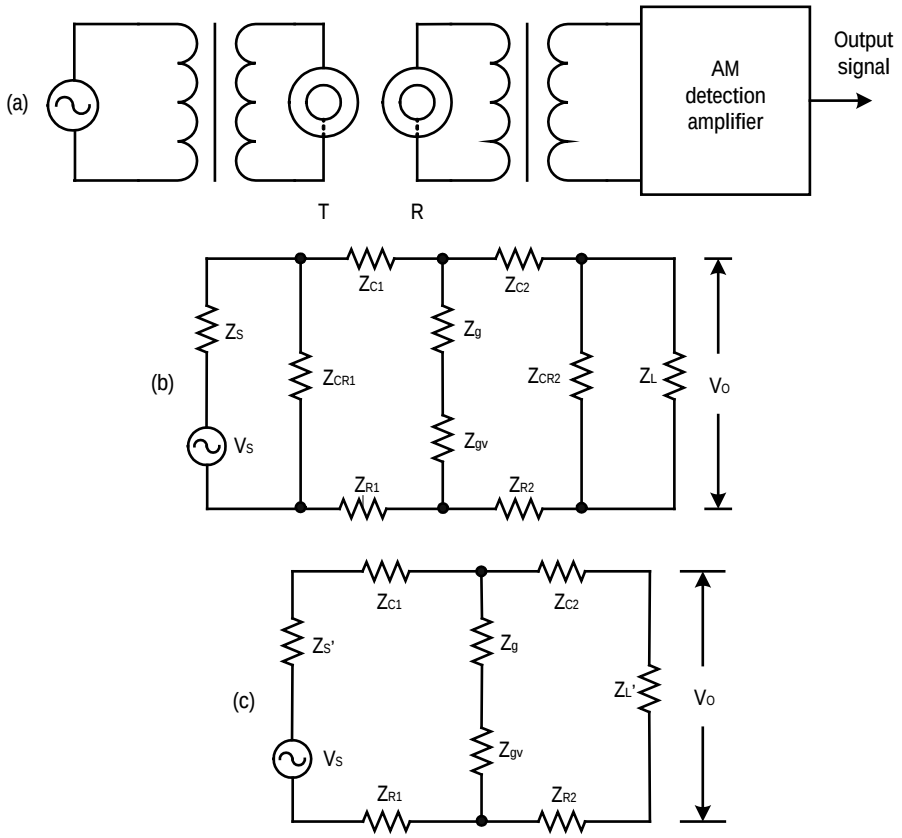

Figure 2.7: (a) Impedance detection method used in instrument patented by Fourcin [40] (b) Equivalent circuit, (c) Reduced equivalent circuit

can be modeled as fixed impedance Z_g in series with time-varying impedance Z_{gv}. Z_s is source impedance, Z_L is input impedance of the detecting circuit and Z_{C1}, Z_{R1}, Z_{C2} and Z_{R2} are the contact impedances of the electrodes CE1, RE1, CE2 and RE2 respectively. Z_{CR1} is the impedance across the skin between CE1 and RE1, and Z_{CR2} is the impedance across the skin between CE2 and RE2. The circuit can be simplified to the circuit of Figure 2.8 (c), Thus,

$$V_O = V_S^{'}\left[\frac{Z_g + Z_{gv}}{Z_S^{'} + Z_{C1} + Z_{R1} + Z_g + Z_{gv}}\right]\left[\frac{Z_L^{'}}{Z_L^{'} + Z_{C2} + Z_{R2}}\right]$$

$$V_S^{'} = \frac{Z_{CR1}}{Z_S + Z_{CR1}} V_S$$

$$Z_S^{'} = Z_{CR1} \,||\, Z_S$$

$$Z_L^{'} = Z_{CR2} \,||\, Z_L$$

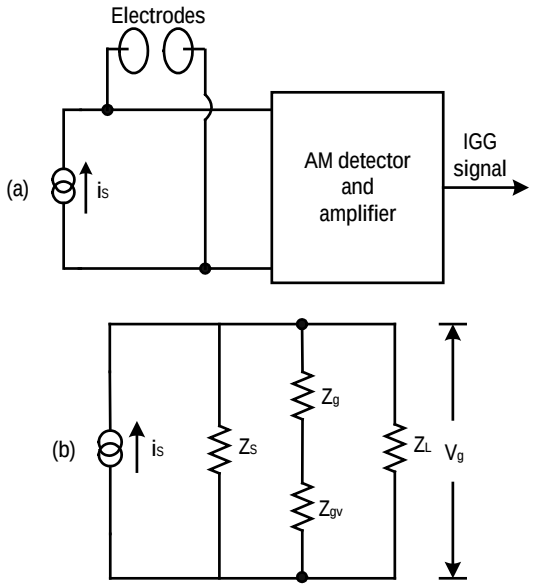

Figure 2.8: (a) Impedance detection method used in the instrument developed at IIT Bombay [23] – [27], (b) Equivalent circuit

This results in output voltage,

$$V_O \approx V_S^{'}\left[\frac{Z_L^{'}}{Z_L^{'}+Z_{C2}+Z_{R2}}\right]\left[\frac{Z_g}{Z_S^{'}+Z_{C1}+Z_{R1}+Z_g}\right]\left[1+z_{gv}\left(\frac{Z_S^{'}+Z_{C1}+Z_{R1}}{Z_g\left(Z_S^{'}+Z_{C1}+Z_{R1}+Z_g\right)}\right)\right] \tag{2.6}$$

Thus, when vocal folds vibrate, Z_{gv} varies and the output gets amplitude modulated.

The impedance detection scheme used in our project is as shown in Figure 2.8 (a). A pair of electrodes is placed in contact with the skin on both sides of the thyroid cartilage. A high frequency voltage signal is converted in to current and is injected. The equivalent circuit of the scheme is shown in Figure 2.8 (b). The impedance between the electrodes can be modeled as fixed impedance, Z_g in series with time-varying impedance Z_{gv}, Z_s is source impedance. When the vocal folds vibrate, Z_{gv} varies and the output gets amplitude modulated. The modulation of the output voltage is directly related to the glottal impedance variation.

$$V_O = I_S\left[Z_S \,\|\left(Z_g + z_{gv}\right)\|\, Z_L\right] \tag{2.7}$$

$$\approx \left(Z_S \,\|\, Z_L \,\|\, Z_g\right)\left[1+\frac{z_{gv}}{Z_g}\right] I_S \tag{2.8}$$

assuming Zgv << Zg and Zg << ZS || ZL. This method gives an output voltage proportional to the time-varying impedance and with a relatively high sensitivity.

2.4 Instrument development

Development work for an impedance glottograph has been carried out at IIT Bombay as part of student project [25]–[30]. Chitnis [26] in 1998 developed a glottal impedance sensor that could detect less than Ω impedance variation usin g ~3 mA sinusoidal excitation of 300 kHz. He also developed data acquisition and LCD graphics display unit. Patil [27] in 2000 modified the hardware and the instrument developed could sense the variation using ~1 mA excitation. He used PC sound card for acquisition, analysis, and display of the glottal waveform. The impedance sensor used Wien-bridge oscillator with FET based amplitude stabilization circuit. To demodulate the waveform, a detector circuit with a precision full-wave rectifier and a band pass filter were used. A high impedance indicator using comparator verified proper contact at the skin-electrode interface. To test sensitivity and frequency response of the hardware, a glottal impedance simulator was developed, using an astablemultivibrator and analog switches to generate periodic step variation in the impedance. Luthra [28] in 2004 developed hardware with increased bandwidth up to 5 kHz, to acquire electroglottogram waveform effectively and sensitivity of instrument increased keeping noise level low. He used the instrumentation amplifier to remove common mode pick-up. Sarvaiya [29] in 2006 developed analog switches based laryngeal impedance simulator and a glottogram for improving the noise performance. The waveform generator IC MAX038 was used in place of Wien-bridge oscillator to improve amplitude stability. An operational amplifier based voltage-to-current convertor with a high frequency transformer (PT6E) was used to avoid stray current and external pick-up. A second order Butterworth high pass filter followed by fourth order Butterworth low pass filter realized using IC MAX 274 was used to get a bandwidth of 75 Hz–4 kHz [41], [42].

Mandloi [30] in 2011 used a direct digital synthesizer (DDS) to get sinusoidal waveform with high amplitude stability and selectable frequency. Trans-conductance operational amplifier OPA 861 was used for the voltage-to-current conversion with balanced complimentary outputs. The quad SPDT ADG734 along with OPA 861 was used to implement the synchronous demodulator using current steering to achieve

high sensitivity and better noise performance. Another DDS chip was used to generate synchronized square wave with settable delay to serve as the reference input for controlling the switches for synchronous demodulation. For serial data transmission and for isolation between the instrument and a PC or a computing device used for control and signal acquisition, a 4-channelisolator IC ISO7241A was used.

Several aspects of the earlier design have to be examined to develop an enhanced instrument. The voltage-to-current converter circuit needs to be thoroughly examined. Sensitivity and linearity of demodulator need to be evaluated. After testing of the circuit blocks individually, complete assembled circuit along with software needs to be tested and calibrated. This requires the use of a glottal impedance simulator.

Chapter 3

BIOIMPEDANCE SIMULATOR

3.1 Overview

A bioimpedance simulator can be used for testing sensitivity, linearity, and dynamic response of a bioimpedance measuring instrument. It can also be used for studying the effect of common mode interference on the measurement. In our application, the bioimpedance can be modeled as a time-varying resistance. For finding the dynamic response of the instrument, variation in the simulated bioimpedance can be in the form of a sinusoidal, triangular, or a square wave. As generating a step change in resistance is simpler and the square wave response can be used for obtaining the transient and frequency response [33], a square wave variation in the resistance with a selectable frequency is used.

A simulator developed earlier [27] used astable multivibrator with a potentiometer to control the frequency and analog switches to change the resistance. Sarvaiya [29] used a microcontroller for generating the square wave and controlling the analog switches. LCD and two keys interfaced to the microcontroller were used for setting the simulation parameters. This design reduced the wiring related pickups and improved the operational flexibility. Mandloi [30] redesigned the simulator by using a digital potentiometer along with fixed R network for simulating the resistance variation. The frequency, base resistance, and the change in resistance were set using four keys and LCD interfaced to the microcontroller. The circuit provided four different basal resistances in the range of 30–40 Ω and a frequency range of 75–500 Hz.

A bioimpedance simulator using a microcontroller, analog switches, and a digital potentiometer has been developed and prototyped. It provides a digital control of basal resistance and a precise control of the change in basal resistance. An increase in the number of basal resistances in the range 10–160 Ω makes the simulator usable for testing different bioimpedance measuring instruments. The simulation parameters are set through an isolated serial interface. The circuit is powered by a battery which

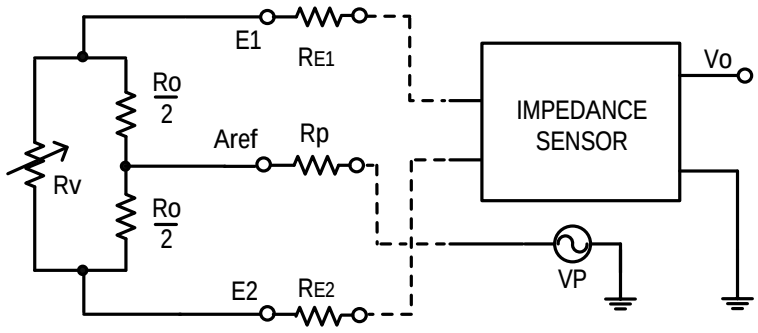

Figure 3.1: A model of the impedance simulator.

can be charged using a USB connector. It can also be powered directly through the USB connector. The circuit is designed in association with Desai [34].

3.2 Bioimpedance model

The time-varying bioimpedance, with 2-electrode measurement setup can be modeled by a resistive network as shown in Figure 3.1 [37]. The terminals E1 and E2 represent the electrode contact points. Resistance R_o is the fixed resistance and R_v represents resistance variation due to physiological effects or internal artifacts. Resistances R_{E1} and R_{E2} represent the electrode-tissue contact impedances. The common mode interference due to internal bioelectric sources or external pickup is represented by V_p in series with resistance R_p, connected between the reference point Aref and the ground of the impedance sensing instrument. The resistance R_p represents the impedance of the common-mode pickup path. The equivalent resistance across E1 and E2 is given by,

$$R_e = R_o \,||\, R_v \tag{3.1}$$

For being useful, a bioimpedance simulator should have the base resistance and the variation in the resistance settable over a large range. We need the basal resistance in the 10–160 Ω range and the square wave variation in the resistance with a settable frequency of 0.1–1000 Hz. Both operations can be achieved by using a digital potentiometer. As digital potentiometers currently available have a wiper resistance of about 50Ω, they cannot be used for setting the base resistance. We can use a resister network and analog switches for selecting the value of the base resistance, by using switches having on resistance much lower than 0.5 Ω. A series

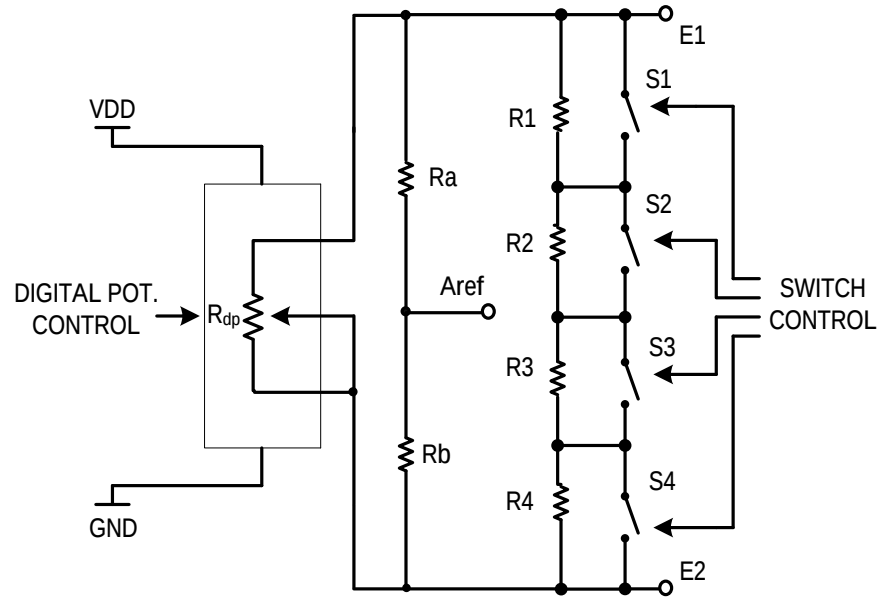

Figure 3.2: Schematic of bioimpedance simulator circuit.

connection of resistors, each paralleled by an analog switch provides maximum flexibility in selecting the values. A resistor network with four analog switches is used, because four analog switches are generally available in one IC. The digital potentiometer used should have a value much larger than its wiper resistance and it can be connected in parallel with base resistance to realize small changes.

The schematic of a bioimpedance simulator for the impedance model of Figure 3.1 is shown in Figure 3.2. The basal resistance is realized using a resistive network and analog switches. The switches S_1–S_4 are operated in different combinations for selecting different basal resistance values. Variation in the resistance is achieved by the digital potentiometer, R_{dp}. The equivalent resistance across the terminals E1 and E2 is given by,

$$R_{E1E2} = R_{sw} \,||\, (R_a + R_b) \,||\, R_{dp} \tag{3.2}$$

where, R_{sw} is the resistance obtained by control of the combination of resistors R_1, R_2, R_3, R_4 through the analog switches. An internal reference of 1.65 V is used as A_{ref}. The signal across the digital potentiometer is with respect to A_{ref}.

3.3 Block diagram of the simulator

A block diagram of the impedance simulator is shown in Figure 3.3. It consists of an analog switch and R-network in parallel with a digital potentiometer, controlled by a microcontroller for setting the base resistance and variation in resistance.

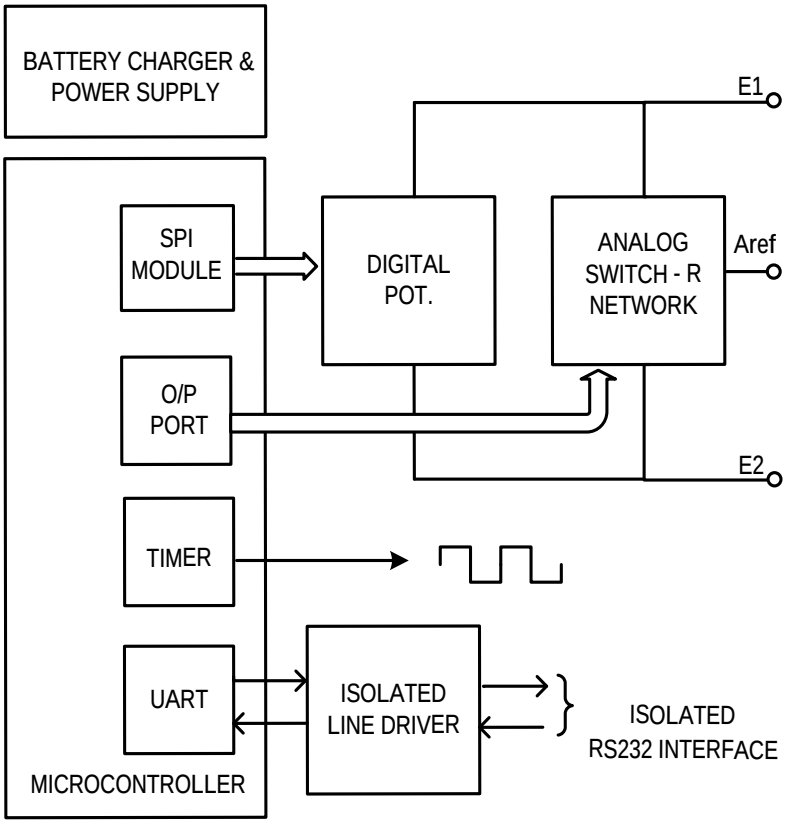

Figure 3.3: Block diagram of bioimpedance simulator.

The simulated resistance is obtained across terminals E_1 and E_2. Square wave of the desired frequency is generated using the on-chip programmable counter/timer of the microcontroller. The settings are controlled by the serial port, using PC or some other external controller for user interface. Isolated RS232 driver is used for providing isolation between simulator and the user interface.

3.4 Hardware blocks

The simulator is realized using a digital potentiometer and analog switches and resistors, all controlled by a microcontroller. Different basal resistances can be selected by the analog switches. The resistance of the digital potentiometer is varied as a square wave by sending the digital control word to its serial register. The values of the basal resistance, variation in the resistance, and the frequency are set through the isolated serial port, to avoid any common mode interference due to user interfacing.

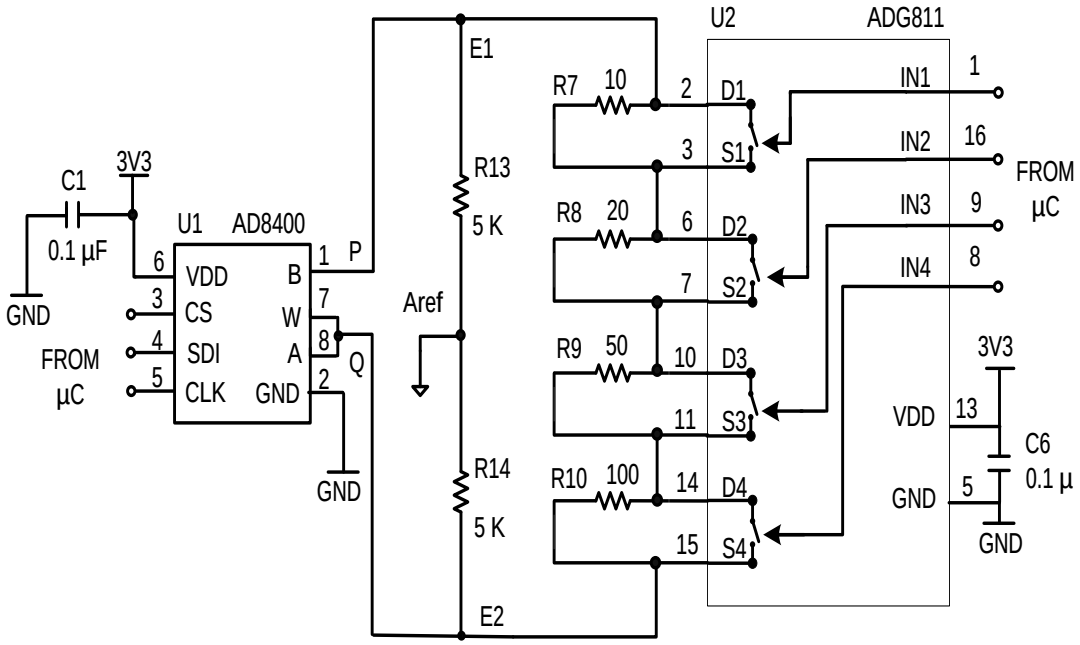

Figure 3.4: Circuit of the resistance variation part of the simulator using the digital potentiometer and analog switches.

3.4.1 Resistance variation circuit

The resistance variation circuit is realized using the digital potentiometer AD8400 (Analog Devices) [38], used here as U1, and quad analog switch ADG811 (Analog Devices), used here as U2 as shown in Figure 3.4. The digital potentiometer has a resistance of 1 kΩ which can be varied in 256 steps from 0 Ω to 1 kΩ. Each step change of digital potentiometer changes its resistance by 4Ω. The wiper resistance of AD8400 is approximately 50 Ω. The change in resistance of digital potentiometer in parallel with the basal resistance is used to get overall resistance change of ≈ 0.1 Ω. The digital potentiometer operates at 3.3 V supply voltage with maximum supply current of 1 mA.

The on-resistance of quad analog switch U2 is less than 0.5 Ω. It operates at supply voltage of 3.3 V with maximum supply current of 0.5 mA. Resistors R_7–R_{10} along with different combinations of switches can be used to get 16 nominal resistance values over 0–180 Ω as given in Table 3.1. The circuit formed by the switches and resistors is and connected in parallel with the variable digital potentiometer resistance R_{dp}. The resistance across E_1 and E_2 is given by,

$$R_{E1E2} = R_{dp} \,||\, (R_{13} + R_{14}) \,||\, R_{sw} \tag{3.3}$$

Table 3.1: Resistance values (nominal) for different switch combinations

Switch control				Resistance
S1	S2	S3	S4	R_O (Ω)
0	0	0	0	0
1	0	0	0	10
0	1	0	0	20
1	1	0	0	30
0	0	1	0	50
1	0	1	0	60
0	1	1	0	70
1	1	1	0	80
0	0	0	1	100
1	0	0	1	110
0	1	0	1	120
1	1	0	1	130
0	0	1	1	150
1	0	1	1	160
0	1	1	1	170
1	1	1	1	180

where R_{sw} is given as $R_{sw} = S_1R_7 + S_2R_8 + S_3R_9 + S_4R_{10,}$ the value of S_1, S_2, S_3 and S_4 is 0 if the corresponding switch is closed and 1 if it is open. The resistance of the digital potentiometer is set by digital control word transmitted to its serial register from the microcontroller via SPI interface.

With S_1 and S_3 closed and S_2 and S_4 open, we get, R_{sw} = 60 Ω. For R_{dp} = 312 Ω the resistance across electrodes E1 and E2 is R_{E1E2} = 50 Ω. 312 Ω. With R_{dp} changed to 304 Ω, we get R_{E1E2} = 49.9 Ω, i.e., ΔR = 0.1 Ω. Periodic change in the resistance is achieved by programming the digital potentiometer periodically at the set frequency.

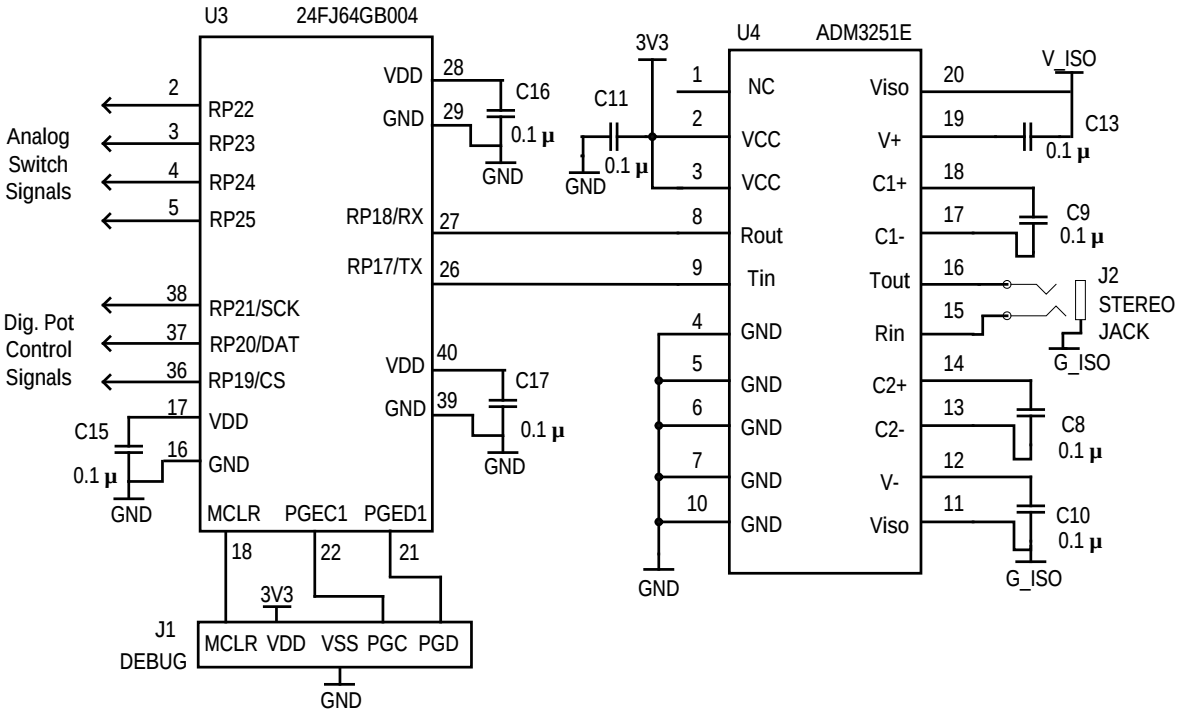

Figure 3.5: Microcontroller and serial line driver interconnection.

3.4.2 Microcontroller and isolated serial interface

The microcontroller PIC24FJ64GB004 (Microchip) [8] is used here as U3. It has 4 programmable counters/timers, 2 SPI modules, 2 UART modules and an in-built USB module. The maximum operating clock frequency of the microcontroller is 32 MHz. Internal RC oscillator with PLL is used for generating clock, eliminating the use of external clock or crystal. The microcontroller operates at 3.3 V supply voltage, with maximum supply current of 16 mA. The digital potentiometer is controlled using SPI module, the analog switches are controlled via general purpose I/O pins, and RS-232 line driver is connected via UART 0 module.

The parameters of the bioimpedance simulator are set through the serial interface between microcontroller and a PC or an external device. Serial interface is established using an isolated single channel RS-232 line driver ADM3251E (Analog Devices) used as U4. It operates at 3.3 V supply voltage on the primary side (microcontroller side) with maximum supply current of 5 mA and 5 V on the secondary side (PC side) with maximum supply current of 12 mA. It is powered by a USB connector on the secondary side. Alternatively, it can be operated with a single supply, connected at the primary side. Its internal isolated dc-dc converter can be enabled by not connecting the external 5 V supply (V_ISO). This method is not used as large current (140 mA) is

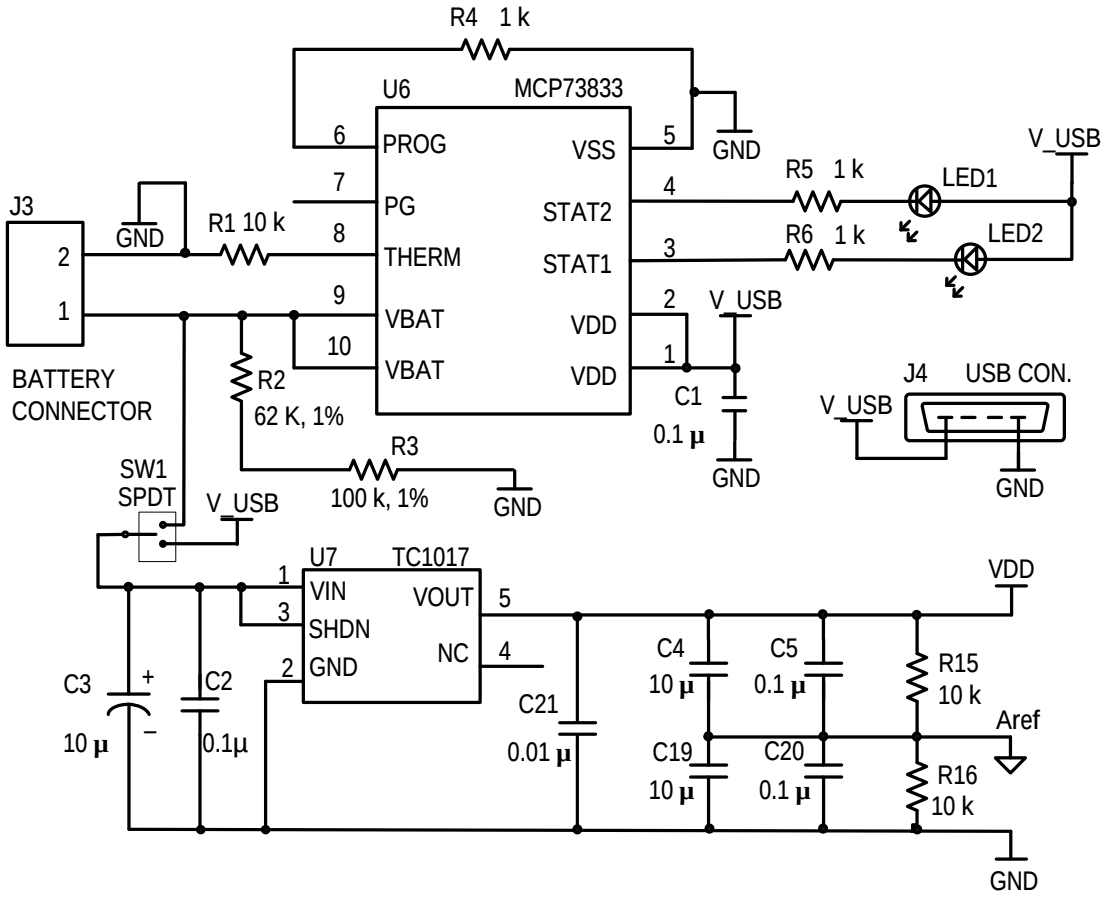

Figure 3.6: Power supply circuit with battery charge management controller MCP73833.

drawn from the primary side. Simulation parameters are set using a cable with stereo jack connector J2 on the microcontroller side and DB9 connector on the PC side.

3.4.3 Power Supply

All the components used in the circuit can operate at supply voltage of 3.3 V. A single linear regulator with required current rating and low dropout voltage is used for powering all the components. The maximum current drawn by the circuit, estimated as the sum of the currents of individual components (digital potentiometer U1: 1 mA, quad analog switch U2: 0.5 mA, microcontroller U3: 16 mA, primary side of the isolated serial driver U4: 5 mA), is 22.5 mA. A low dropout regulator chip TC1017–3.3VLT is used as U7 as shown in Figure 3.6. It can deliver up to 150 mA of current with quiescent current of 90 µA. It has operating input range of 3.58–5.63 V at maximum load current of 150 mA. For load current of 22.5 mA, the input voltage range is 3.58–6.4 V with maximum power consumption of 61 mW.

A Li-Ion battery with output voltage of 4.2 V when fully charged is used for powering the regulator. Charge capacity of a typical Li-Ion battery is about 1200 mAh. The charger circuit, as shown in Figure 3.6, consists of a stand-alone linear Li-Ion charge management controller MCP73833 (Microchip) used as U6. It can operate with supply voltage of 4.5–6 V with quiescent current of 3 mA. Temperature sensing of U6 is disabled and a 10 kΩ register is connected to THERM as recommended in the datasheet. LED1is used to indicate battery charging and LED2 for indicates whether the battery is fully charged. The board is powered through a USB connector. A double throw switch SW1is used to power the regulator by battery or directly by the USB connector.

Common mode interference rejection of the external circuit can be tested by injecting interference at common mode input point. An internal reference point at 1.65 V with respect to GND is provided to simulate common mode input point.

3.5 Software

The digital potentiometer U1 is controlled by the microcontroller via SPI interface and the quad analog switch U2 is directly connected to the I/O port of the microcontroller. The microcontroller also communicates with the PC for setting the simulation parameters via UART 0. The program involves simulating the change in basal resistance at a given frequency based on the set values of R and ΔR. The algorithm is described as below.

Main Program

1. Configure serial port.
2. Set timer1 configure bits.
3. Set the default values of digital potentiometer and analog switch.
4. Load timer registers with the counts according to the set default frequency.
5. Update the simulation parameters when the serial interrupt occurs.

Interrupt Service Routine

If the interrupt is due to timer, do the following.

1. Reload the timer registers.
2. Update digital potentiometer register by the specified value from the look-up table.

3. Invert the SYNC pin to generate square wave.
4. Return.

If the interrupt is due to serial byte reception, do the following.

1. Decode the received byte and set the different parameters.
2. Update the analog switch controls.
3. Return.

3.6 Assembly and testing

The component list is provided in Appendix A. The complete schematic of the bioimpedance simulator is given in Appendix B. A double sided PCB with PTH was designed for the impedance simulator. Size of the PCB is 73 mm x 61 mm. Components are populated on one single side of the PCB. Supply plane is provided on the top layer and ground plane on the bottom layer to reduce the external noise. Care is taken to minimize the length of the supply track for ICs. Supply for each IC is decoupled by 0.1μF capacitors placed as close as possible to the ICs. Most of the components including resistors and capacitors are in SMD packaging. The component placement with track layout is given in Appendix C.

3.7 Test results

The resistance values were measured using a multimeter (HP34401A) across terminals E1 and E2 as shown in Figure 3.2. For different combination of switch positions and digital potentiometer values, basal resistances (R) along with change in resistance (ΔR) obtained are tabulated in Table 3.2. R_{dp1} and R_{dp2} are the digital potentiometer values used to get the basal resistance and change in resistance at the set frequency. The measured values show a good match with the nominal values.

Table 3.2 Basal resistance R (Ω) and change in resistance ΔR (Ω)

Switch status				Digital pot. value		Resistance across E1 – E2			
						Nominal		Measured	
S1	S2	S3	S4	R_{dp1} (Ω)	R_{dp2} (Ω)	R (Ω)	ΔR (Ω)	R (Ω)	ΔR (Ω)
0	1	1	0	160	36	10.00	0.50	9.99	0.49
0	1	0	0	88	64	20.00	0.50	19.98	0.50
1	1	0	0	920	600	30.00	0.50	29.95	0.52
1	1	1	0	312	272	50.00	0.50	50.00	0.55
1	0	0	1	608	540	60.00	0.50	60.07	0.52
0	1	0	1	600	552	70.00	0.50	70.03	0.52
1	1	0	1	212	52	80.00	0.50	80.01	0.55
0	1	1	1	484	464	100.00	0.50	100.02	0.53
0	1	0	1	644	604	120.00	0.50	120.01	0.52
1	0	1	1	844	824	160.00	0.50	159.88	0.53

Chapter 4

IMPEDANCE GLOTTOGRAPH

4.1 Introduction

A block diagram of impedance glottograph, to monitor the degree of contact between the vibrating vocal folds, is shown in Figure 4.1. It consists of sinusoidal source, voltage-to-current converter, voltage sense amplifier and demodulator. Impedance is sensed by generating an excitation signal in the frequency range of 50–500 kHz. This signal is provided to a voltage-to-current converter to output a low amplitude (< 5 mA) current, which is injected using a pair of electrodes held in contact with the skin on both sides of the thyroid cartilage. The resulting amplitude modulated signal is amplified using a voltage sense amplifier and given to the demodulator. The output waveform of the demodulator represents the impedance variation, and is known as the impedance glottogram or electroglottogram or laryngogram.

Excitation signal is generated using Direct Digital Synthesizer (DDS) which provides digital control of the frequency and high amplitude stability. The complementary outputs of the DDS are given to a differential amplifier. The output of the amplifier is fed to a voltage–to–current converter for constant current output, and to the demodulator for baseline restoration. Two outputs with amplitude controls are achieved using two digital potentiometers.

The current output from the voltage-to-current converter is injected on the skin on both sides of the thyroid cartilage through electrodes I1 and I2. The impedance across the electrodes is primarily resistive for the excitation frequency in the range of 100 kHz to 1 MHz. The impedance is typically in the range of 100 to 500 Ω, and the time-varying component is much less than 1 Ω [19]. The amplitude modulated signal due the change in degree of contact between the vibrating vocal folds is sensed by an instrumentation amplifier. As the time-varying component of the impedance is low (<<1 Ω), a demodulator with very high noise rejection, high sensitivity, and low carrier ripple is needed. Further to preserve the waveshape of the sensed signal,

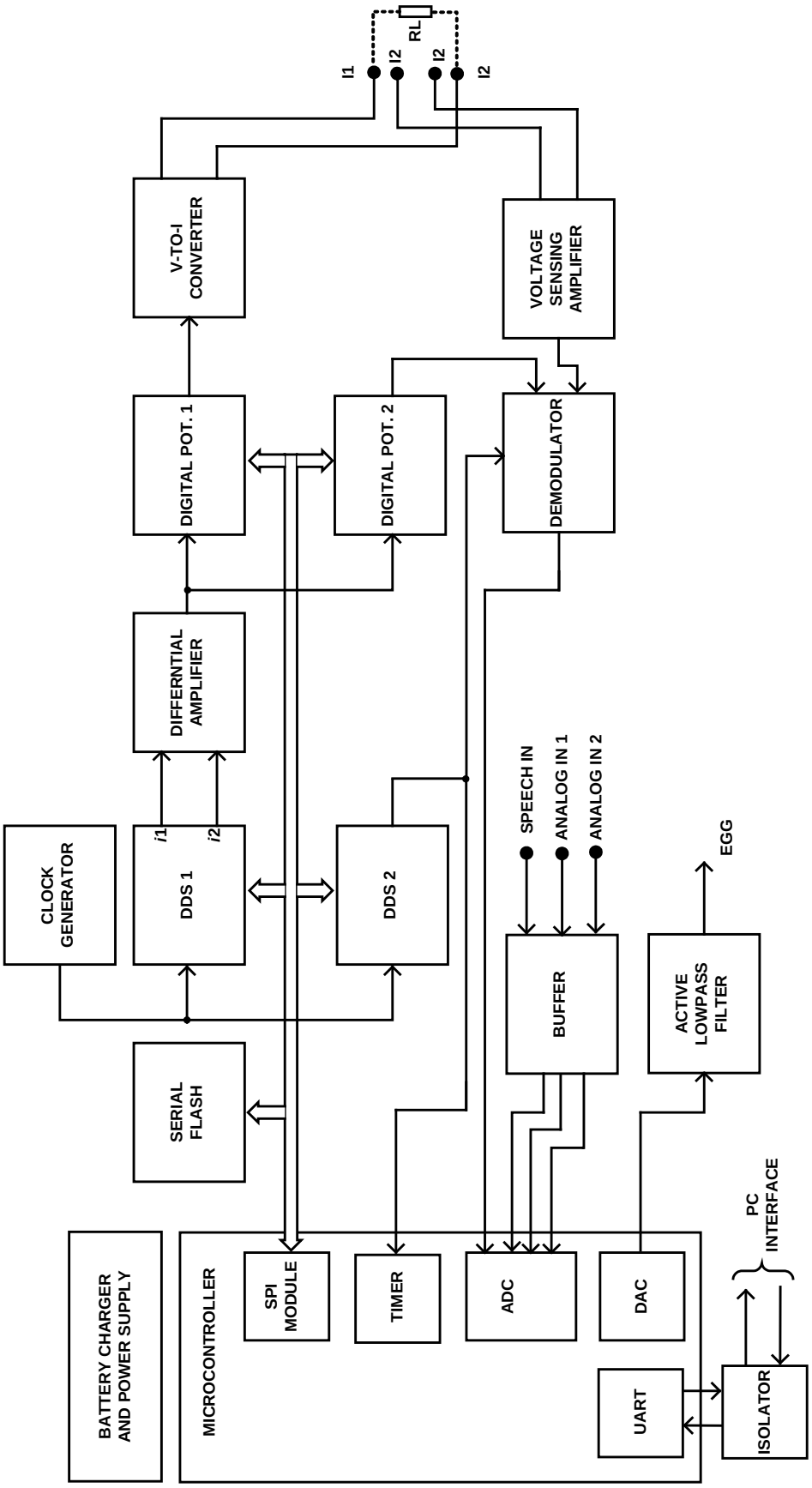

Figure 4.1: Block diagram of the impedance glottograph device

a demodulator circuit with low phase distortion is needed. It is designed to achieve synchronous demodulation for extracting the impedance variation *z(t)* from the amplitude modulated output of the instrumentation amplifier. There is a provision to connect three external analog inputs for flexibility in the application of the instrument. These inputs along with *z(t)* are sampled by in-built ADC of the microcontroller. User settings are controlled by a PC or some other external device which is connected to the microcontroller through an isolated RS232 driver.

4.2 Excitation source

The excitation source consists of a waveform generator, amplitude control circuit and voltage-to-current converter. Frequency and phase of the waveform regenerators along with the amplitude of the current output of the voltage-to-current converter are controlled by the microcontroller.

4.2.1 Waveform generator

A sinusoidal source with high amplitude stability is required, as any instability in the waveform generator would contribute to the noise in the output, resulting in a corrupted glottogram signal. A sinusoidal source with amplitude instability of lower than 0.1% is preferred. Hence a direct digital synthesizer with precise control over frequency and phase is used as a stable waveform generator. The DDS AD9834 (Analog Devices) [39] is used as U2 and U3. It can produce accurate sinusoidal, triangular and square waveforms using samples stored in its on-chip memory. The frequency and the phase of the output are controlled by sending the required count words to its 24 bit frequency and 12 bit phase registers respectively. The output frequency and phase are given by,

$$f_{\text{out}} = f_{\text{MCLK}} \; N_{\text{FREQREG}} / 2^{28} \tag{4.1}$$

$$\theta_{\text{out}} = 2\pi \; N_{\text{PHASEREG}} / 2^{12} \tag{4.2}$$

where, $N_{FREQREG}$ and $N_{PHASEREG}$ are the counts loaded in the frequency and the phase registers of the DDS and f_{MCLK} is the master clock frequency given to the DDS. The DDS can generate output waveform with maximum frequency of f_{MCLK}/2. The chip can be reset either by software or hardware. Software reset is achieved by setting

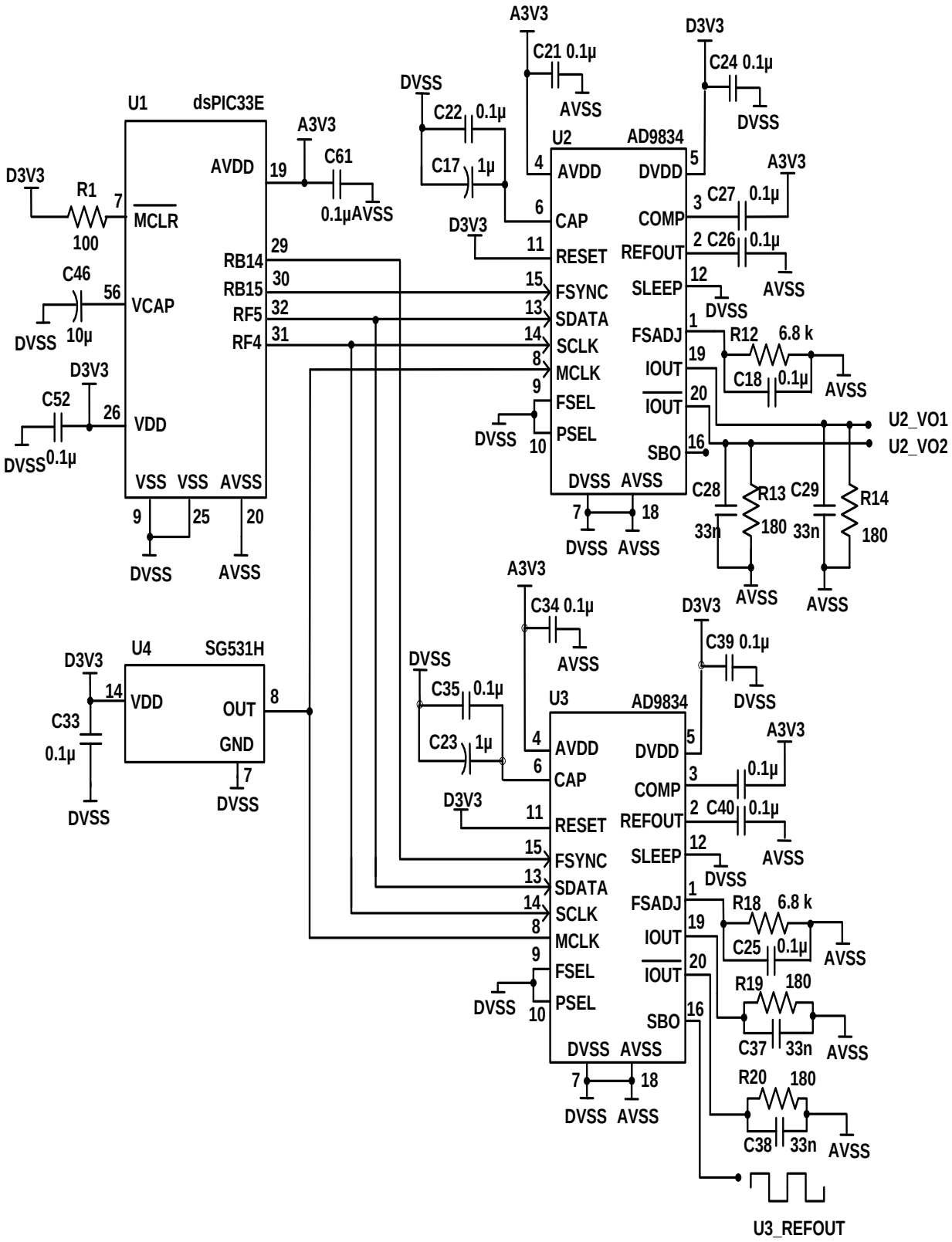

Figure 4.2: Controller circuit for the waveform generator

appropriate bit in the control register and hardware reset is achieved by setting the RESET pin from high to low. The device can be controlled by SPI interface with maximum clock frequency of 40 MHz. This synthesizer has two complementary unipolar current outputs. The amplitude of the current can be controlled by connecting an external resistor from FSADJ pin to the ground and the current is given by,

$$i_{out} = 18\ V_{refout} / R_{set} \tag{4.3}$$

where, R_{set} is the resistance connected between pin FSADJ and ground, V_{refout} is the internally generated constant reference voltage, equal to 1.2 V and is provided on pin 2 of the DDS. The voltage generated across the resistor R_{set} should not exceed 0.8 V.

In our design, two DDS chips U2 and U3 are used. Both are clocked by a single crystal oscillator SG531H used as U4, with output clock frequency of 40 MHz. U2 and U3 are connected to the microcontroller U1 dsPIC33EP256MU806 via SPI interface. Both the DDS chips have their SDATA and SCLK pins connected in common to the microcontroller. Their FSYNC pins are connected separately to the microcontroller and used as chip select for transferring the data. A resistance of 6.8 kΩ is connected to FSADJ pin to provide an output current of 3.17 mA. Resistors are connected between the two output pins and the ground to convert the current output to voltage, as shown in Figure 4.2. The voltage across these resistors should not exceed the compliance limit of 0.8 V. Two resistors of 220 Ω are used to convert current to voltage, resulting in peak-to-peak output of 0.7 V. The maximum current drawn by each DDS is 8 mA. The output of the first DDS (U2) is connected to the differential amplifier and output of the U3 is used for synchronous demodulation which is discussed later. They are operated in the frequency range of 100–500 kHz. Two DDS are synchronized by simultaneously setting the control bit in the control resistor. The FSYNC pin is used as chip select pin for selecting the individual DDS chips.

4.2.2 Amplitude control circuit

The input voltage levels at the voltage-to-current converter and the baseline correction circuit need to be independently set. The complementary outputs of the DDS (U2) are given to the differential amplifier. The output of the differential amplifier is fed to two digitally controlled potentiometers to obtain two independent output voltages which

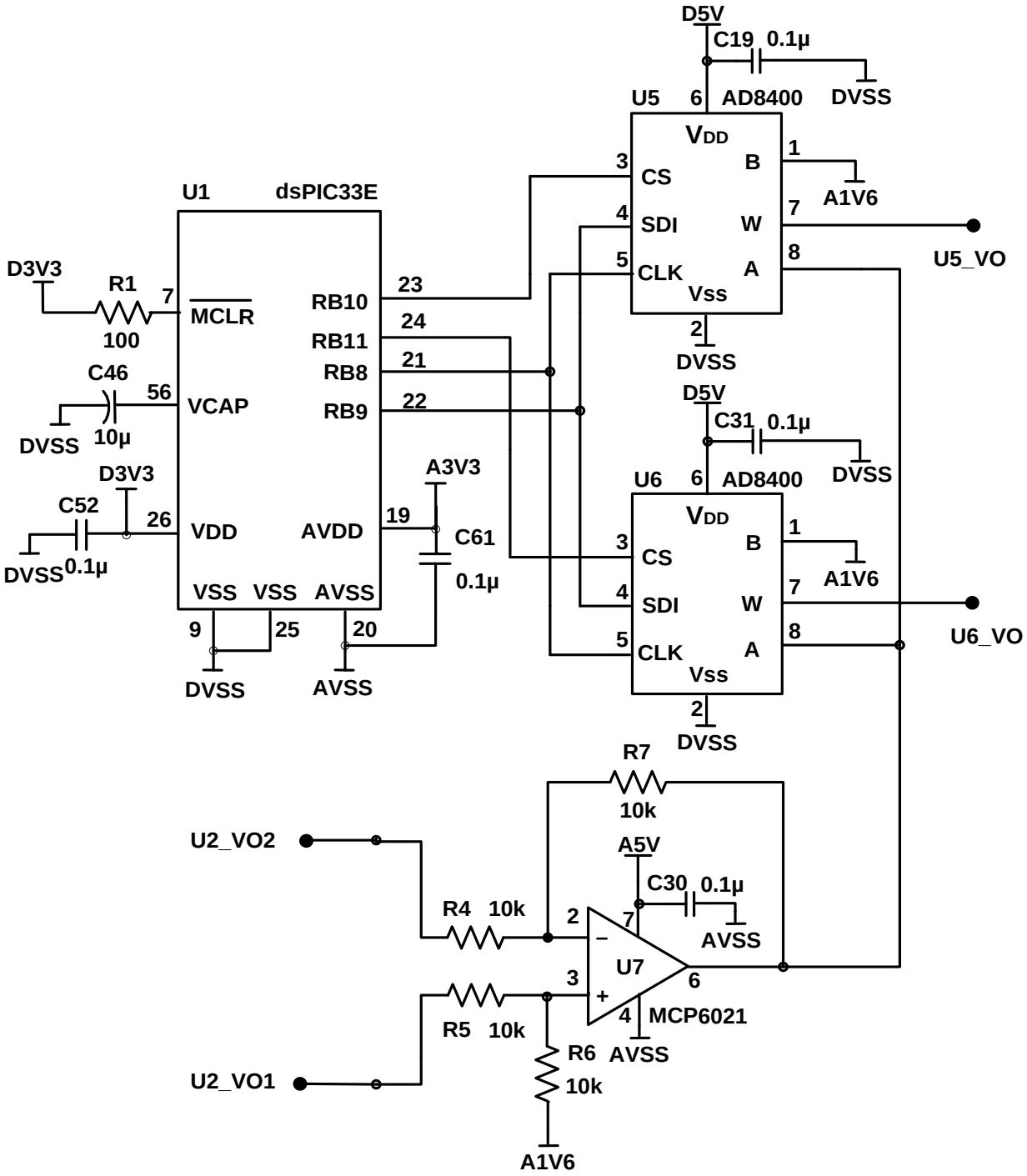

Figure 4.3: Amplitude control circuit using digital potentiometers.

are provided as input to the voltage-to-current converter and the baseline correction circuit. The amplitude control circuit is shown in Figure 4.3.

The digital potentiometer AD8400 (Analog Devices) [40] is used as U5 and U6. It has a resistance of 10 kΩ which ca n be varied in 256 steps from 0–10 kΩ. The

wiper resistance of the digital potentiometer is approximately 50 Ω. Each step change of digital potentiometer changes its resistance by 40 Ω. It operates at 3.3 V with maximum supply current of 1 mA.

The complementary outputs of the DDS, used as U2_VO1 and U2_VO2, are given to the differential amplifier U7. The differential amplifier circuit is built using the operational amplifier MCP6021 (Microchip) [41] used as U7. It can be operated with supply voltage in the range of 2.5–5.5 V and has rail-to-rail output voltage swing. The gain bandwidth product of MCP6021 is 10 MHz and it can source or sink current up to 30 mA. U7 is powered from a single supply of 5 V and has a maximum supply current of 2 mA. An analog reference of 1.6 V used as A1V6, is used to bias the input signal so as to get the full swing within the supply range. The gain of the differential amplifier is 1. The output of the differential amplifier is fed to the two digital potentiometers U5 and U6. Both the potentiometers are controlled by the microcontroller via SPI interface. Thus two independent output voltages at pin 7 of digital potentiometer U5 and U6 with digitally controlled levels are achieved.

4.3 Voltage-to-current converter

Voltage-to-current converter (V/I) is used to convert the voltage signal in to a constant current signal. V/I converter should have high output impedance to drive the electrode for injecting a constant current in the laryngeal region. A low amplitude (< 5 mA) sinusoidal current is injected using a pair of electrodes held in contact with the skin on both sides of the thyroid cartilage.

The simplest realization of V/I converter is an operational amplifier based inverting amplifier [42] with the load connected in the feedback as shown in Figure 4.4. The resistor R_b is used to prevent op amp from entering saturation in case of poor tissue-electrode contact. The capacitors C_a and C_b are used to avoid DC current passing through the electrodes. The circuit is unbalanced as one of the electrodes is connected to the virtual ground, and this may lead to possible arise in stray current and common mode pick-up. Sarvaiya [29] used pulse transformer as a high frequency isolation transformer to get an isolated current source, as shown in Figure 4.5, to avoid the effect of stray current and common mode pick-up. Patil [27] designed a

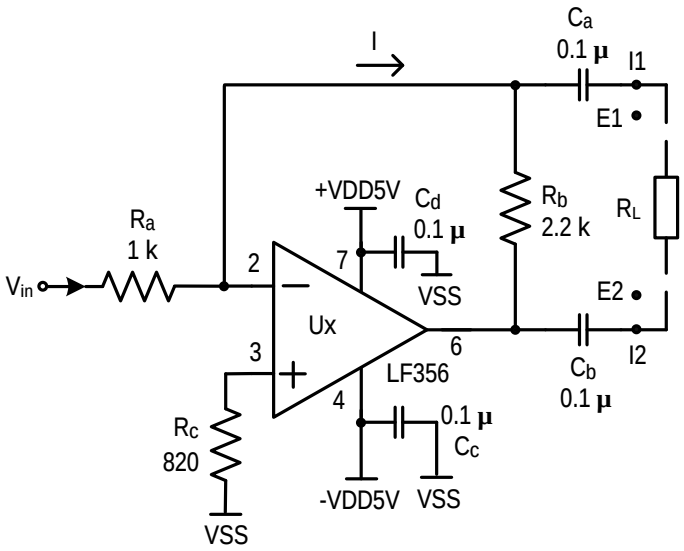

Figure 4.4: V/I converter based on inverting amplifier circuit [46].

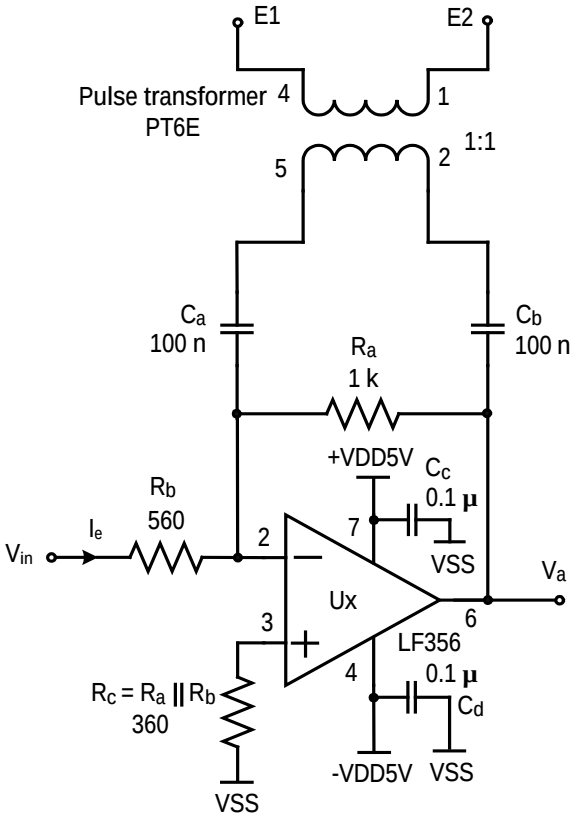

Figure 4.5: V/I converter based on high frequency pulse transformer as used in [29].

transformerless current source using modified Howland circuit, as shown in Figure 4.6. Its advantage is that the output impedance can be made very high by matching the

s

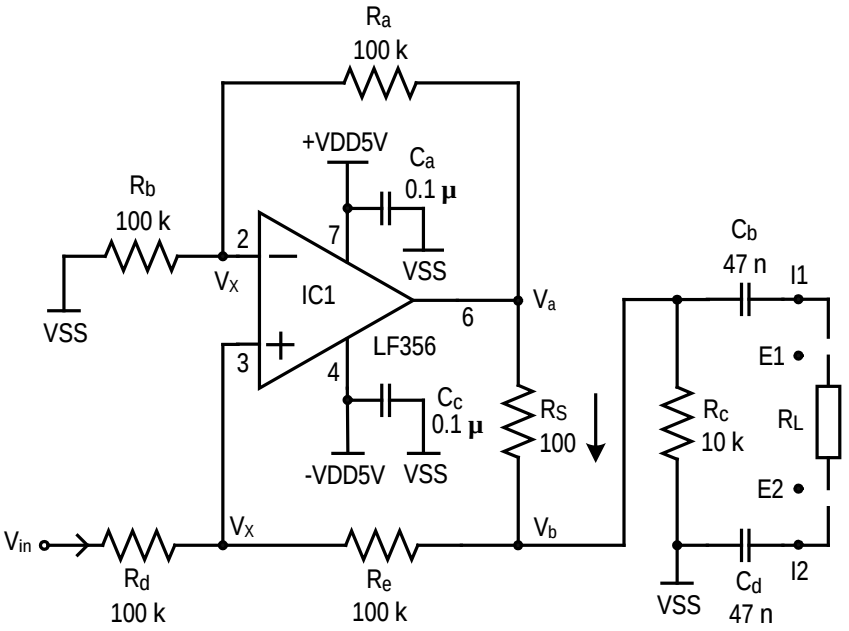

Figure 4.6: V/I converter based on Modified Howland circuit as used in [27].

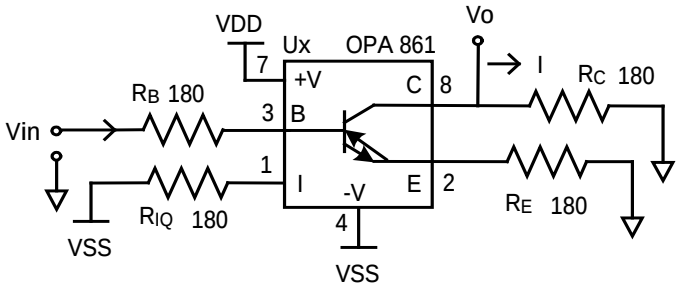

Figure 4.7: Current source using a tans-conductance amplifier.

resistance ratios $R_a/R_b = R_e/R_d$. Instability in the circuit due to stray currents is avoided because one end of the load is connected to ground.

Mandloi [30] used balanced complementary current output design based voltage-to-current converter. The circuit was implemented using trans-conductance amplifiers. The same circuit is used in the present design, because the balanced complementary current output eliminates the need of a transformer. Trans-conductance amplifier OPA 861 (Texas Instruments) [43] is used. It can be operated with single supply of +5 V or at dual supply of ± 5 V. It has a bandwidth 80 MHz, slew rate of 900 V/µs, and trans-conductance of 95 mA/V. The output current *I* of the circuit shown in Figure 4.7 is given by,

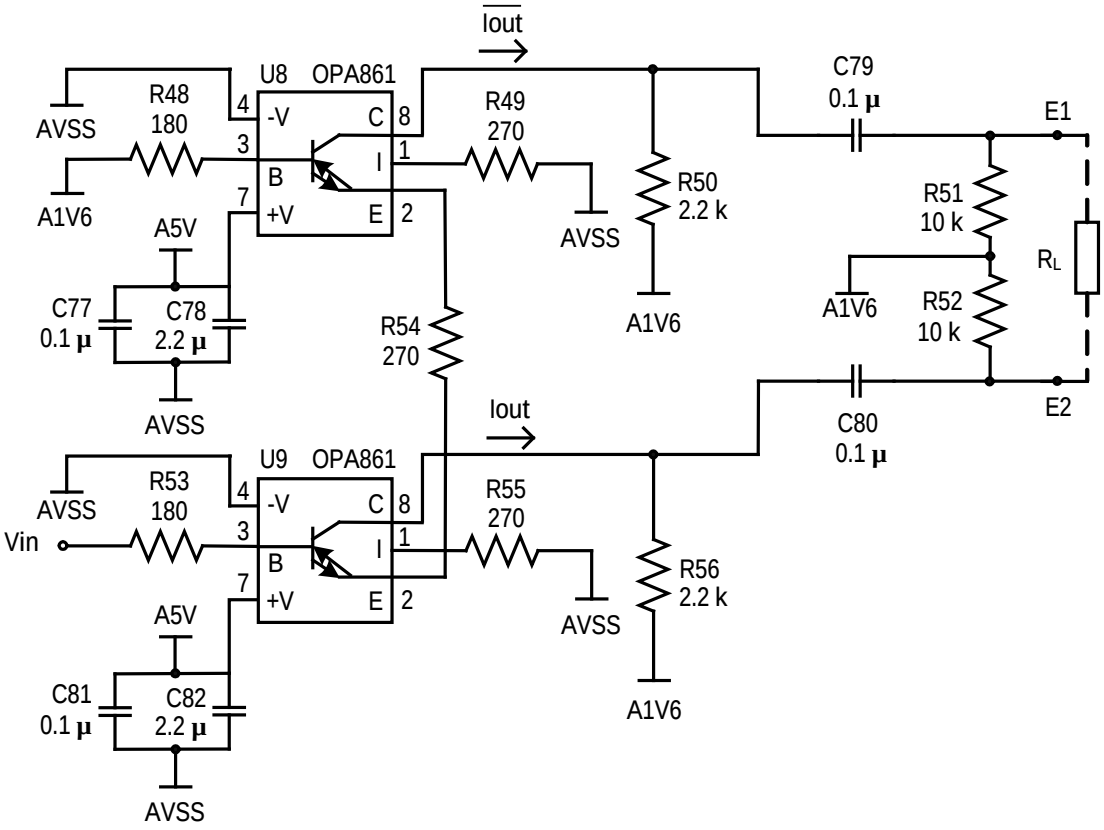

Figure 4.8: V/I converter using trans-conductance amplifier.

$$I = V_{in} / \left(R_E + \left(1 / g_m \right) \right) \tag{4.6}$$

where $g_m$is trans-conductance and R_E is the emitter resistance. The trans-conductance is constant over a wide range of collector currents resulting in higher linearity. The quiescent current is set by connecting the resistor R_{IQ} from pin number 1 to VSS.

Balanced complementary current outputs are achieved by connecting two OPA 861 used as U8 and U9 as shown in Figure 4.8. The voltage waveform is given at the base of U9, while the base of U8 is connected to analog reference A1V6. The quiescent current is set with resistor $220\,\Omega$ connected from pin number 1 to VSS of U8 and U9. The output current is given by

$$I_{out} = \left(V_{in} - V_{aref} \right) / \left(R_{54} + (1 / g_m) \right) \tag{4.7}$$

$$\bar{I}_{out} = -I_{out} \tag{4.8}$$

The complementary current is injected into the larynx through a pair of electrodes. U8 sources the current and the same current is sunk by U9 resulting in balanced

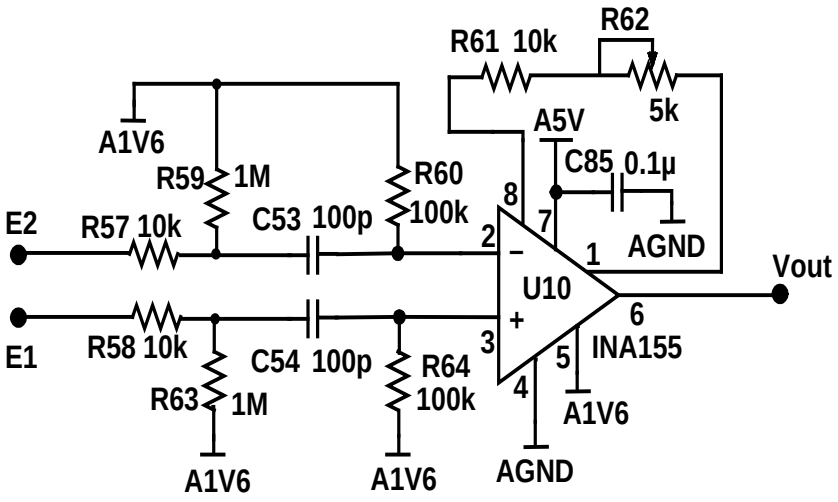

Figure 4.9 Voltage sensing amplifier using IN155.

complementary currents. The magnitude of the current is set by resistor R_{54} as given by the Equation 4.8. Capacitors C79 and C80 are used to block DC current from passing through the electrodes. Resistances R51 and R52 are used for connecting the circuit reference to reduce common mode pickup. Resistors R50 and R56 are used to reduce the effect of any unbalance between the two currents.

4.4 Voltage sense amplifier

The signals obtained from the electrodes are prone to common mode noise. Instrumentation amplifier based circuit can be used to remove such common mode noise pick up. Hence an instrumentation amplifier circuit is used to sense the difference between the voltages developed across the two electrodes placed on either side of the larynx. The instrumentation amplifier INA155 (Texas Instruments) is used as U10. It can be operated with 2.7–5.5 V supply with a current drain of 2 mA. It has a gain bandwidth product of 5.5 MHz, slew rate of 6.5 V/µs and rail-to-rail output swing. The CMRR of INA155 is typically 100 dB. Its gain can be set as 10–50 as,

$$G = 10 + \left(\frac{400\ \text{k}\Omega}{10\ \text{k}\Omega + R_G} \right) \tag{4.9}$$

where, R_G is the resistance connected between pin number 1 and 8 of INA155. In the present design, U10 is operated with 5 V supply and an analog reference A1V6 is connected to pin number 5. The resistor and capacitor network (C45-R64, C53-R60) as shown in Figure 4.9 forms a high-pass filter with cut-off frequency of 16 kHz, given as,

$$f = \frac{1}{2\pi RC} \tag{4.10}$$

where R60=R64=R and C53=C54=C. With R = 100 kΩ and C = 100 pF, we get f = 16 kHz. This helps in rejecting pick-ups without affecting the sensed voltage. This filtered output is given as an input to the instrumentation amplifier. With R61 = 10 k kΩ and R62 = 0 to 5 kΩ, R_G = 10–15 kΩ. A gain of 10 is achieved by not connecting the resistor R62.

4.5 Demodulator

The amplitude modulated signal, due to variation in the laryngeal impedance needs to be demodulated to get the EGG signal. Highly accurate demodulator is necessary as the modulation index of the waveform is in the range of 0.2–2%. Luthra [28] used a full-wave rectifier using operational amplifier. Sarvaiya [29] used a precision rectifier using voltage clamp amplifier IC AD 8037 for demodulation. Patil used a slicing amplifier based demodulator in impedance cardiography circuit [27]. The signal was sliced up to the level of modulation depth and then amplified, for increasing the sensitivity of the demodulator, but it resulted in an increase in carrier ripple. Sampling near the peaks was used in place of a low-pass filter to reduce the carrier ripple, because low-pass filtering introduces phase distortion. Thus circuit achieved high sensitivity and low carrier ripple. However, any noise near the sampling instants contributes to the noise in the output voltage.

Mandloi [30] used synchronous demodulation scheme using current steering. In this design a full-wave rectified signal results at the current summing node as shown in Figure 4.10. Analog switches are controlled by using a square wave synchronous with the sinusoidal carrier. Input components which are synchronous and in phase with the square wave contribute to the output. The load on each voltage source remains constant as current is delivered to the current summing node or to A_{ref}, hence avoiding any discontinuity in the current flow. An ADC is used to sample the output $V_{out,}$ in synchronism with the clock to reject any carrier ripple present in the signal.

Various artifacts due to body movement and analog components in the circuit cause drift in the modulated signal. Therefore, before A/D conversion, drift

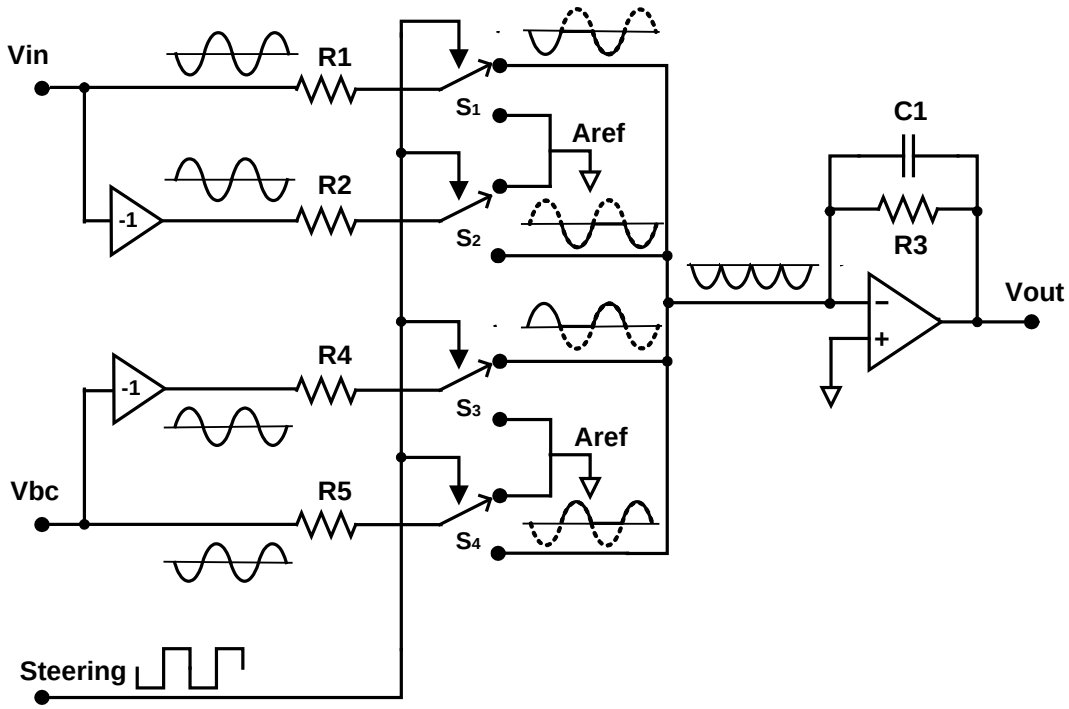

Figure 4.10: Schematic for the synchronous demodulation scheme using current steering.

cancellation using baseline restoration technique has to be carried out to utilize the complete dynamic range of ADC. Demodulated output is used to control the amplitude of the baseline restoration signal V_{bc} and thus to keep the demodulated output within the specified range.

The waveform generated by the DDS1 passes through various blocks before reaching the demodulator, whereas the clock to demodulator is directly from DDS2, resulting in a phase delay between the two. Therefore a phase correction needs to be done by sending appropriate phase word to both the DDSs. The flow chart representing the phase correction logic is shown in Figure 4.11.The phase of the sinusoidal excitation is varied in the range of 0º to 360º with step increment of 5º. At each step increment, ten samples of demodulated output are taken every 100 cycles, averaged and stored in an array. The angle corresponding to the maximum value of the array is taken as the optimum value for the phase correction between demodulator and sinusoidal excitation.

The complementary pair of currents in the demodulator circuit is realized using two trans-conductance amplifiers. A total of four OPA861 are used for realizing

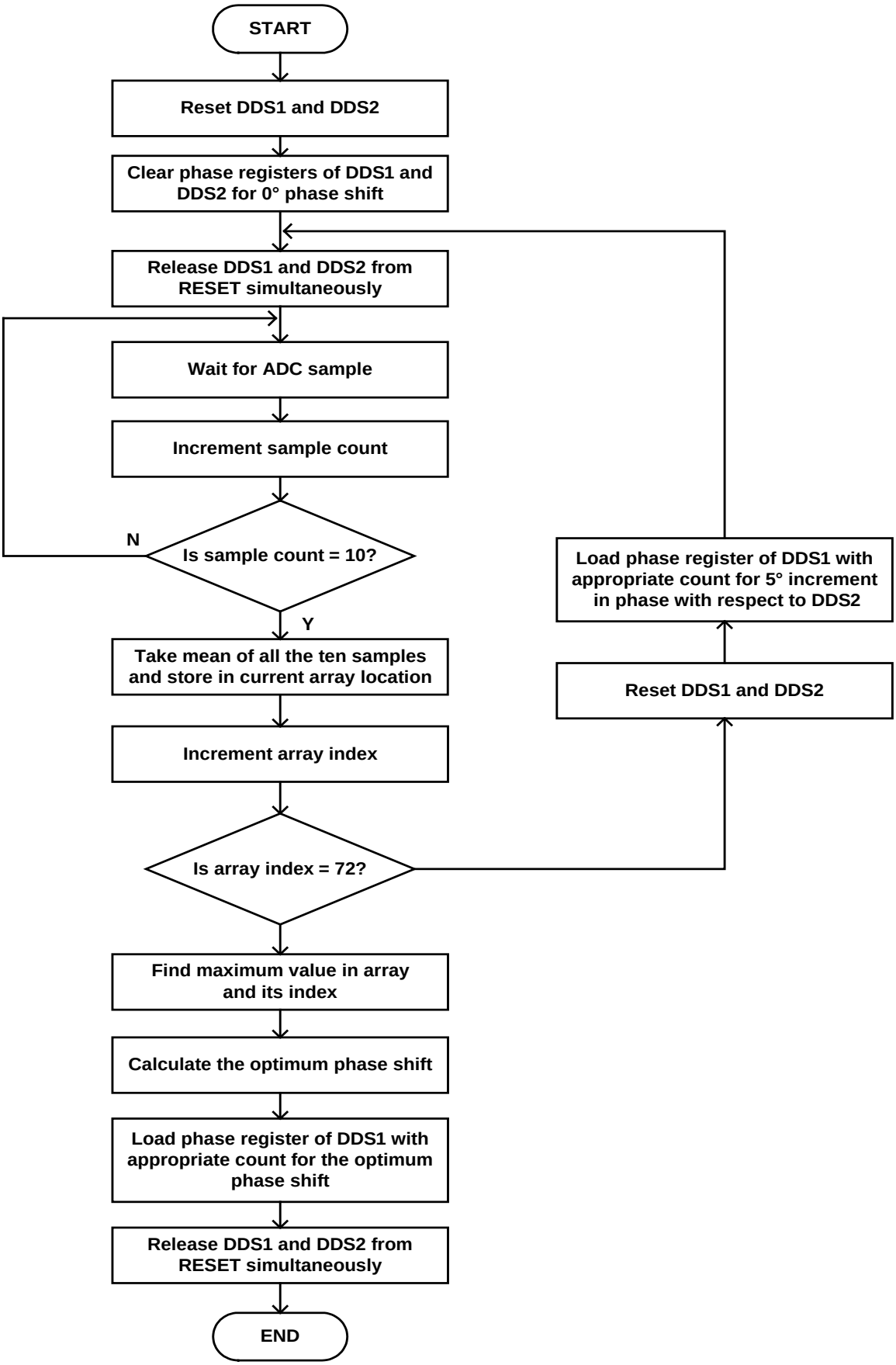

Figure 4.11: Flow chart for phase correction logic.

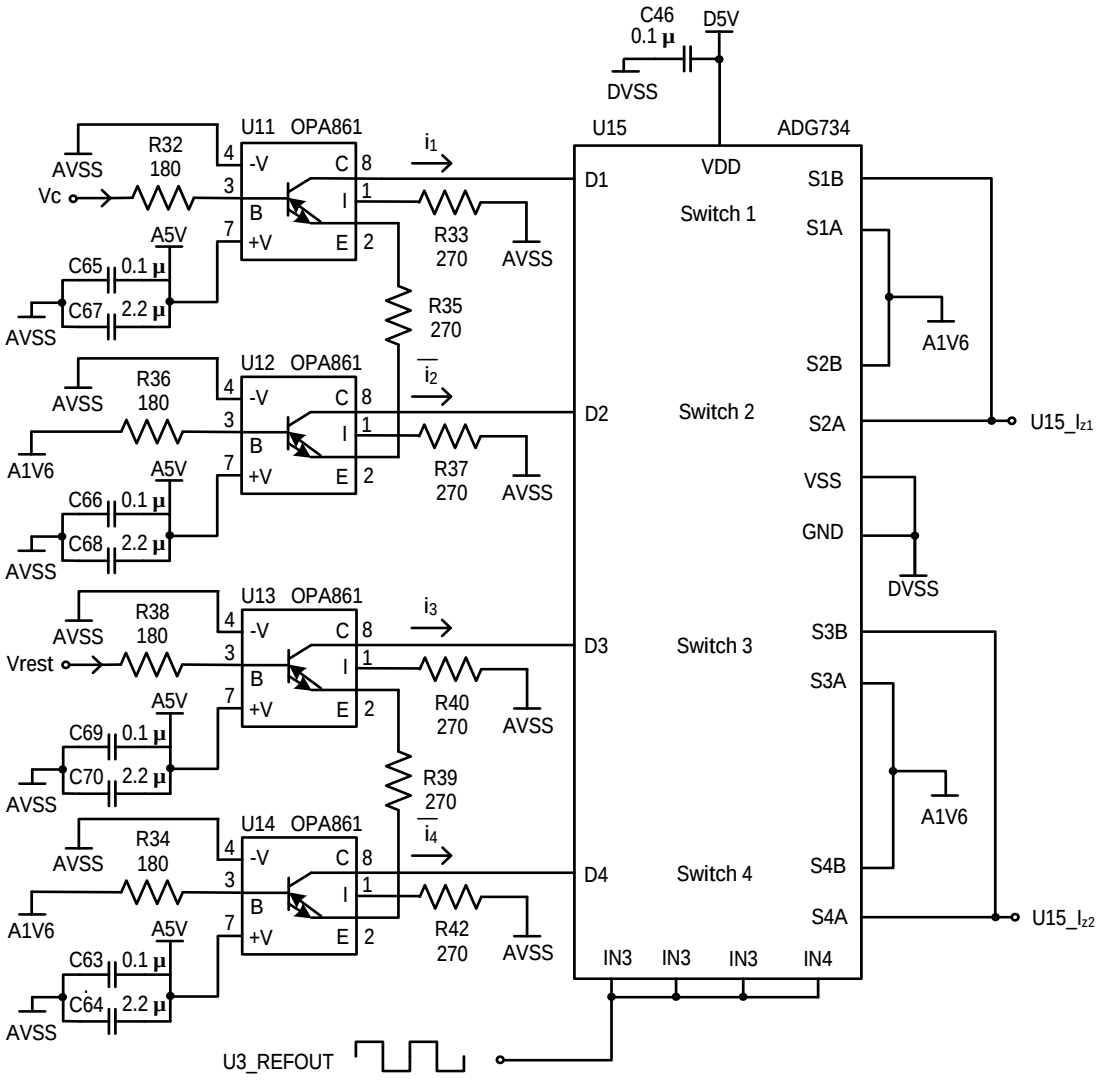

Figure 4.12: Circuit of synchronous demodulation and baseline restoration.

rectification (U11, U12) and baseline restoration (U13, U14) logic, as shown in Figure 4.12. The quad SPDT chip ADG734 (Analog Devices) used as U15, has four independently selectable switches, operates in the supply range of 1.8–5.5 V with rail-to-rail input swing [44]. It has a maximum operating frequency of 160 MHz and has a switching time of 19 ns. All the four SPDT switches are driven by a single clock signal from DDS2. The switches steer the two current outputs in synchronization with the DDS2 clock. The current outputs U15_I_{z1} and U15_I_{z2} from the demodulator and baseline correction circuits are fed to the current summer designed using OPA861, used as U16 as shown in Figure 4.13. The output of the current summer is fed to a second order active low pass filter formed by op amp MCP6012, used as U17. The transfer function of the filter is given by,

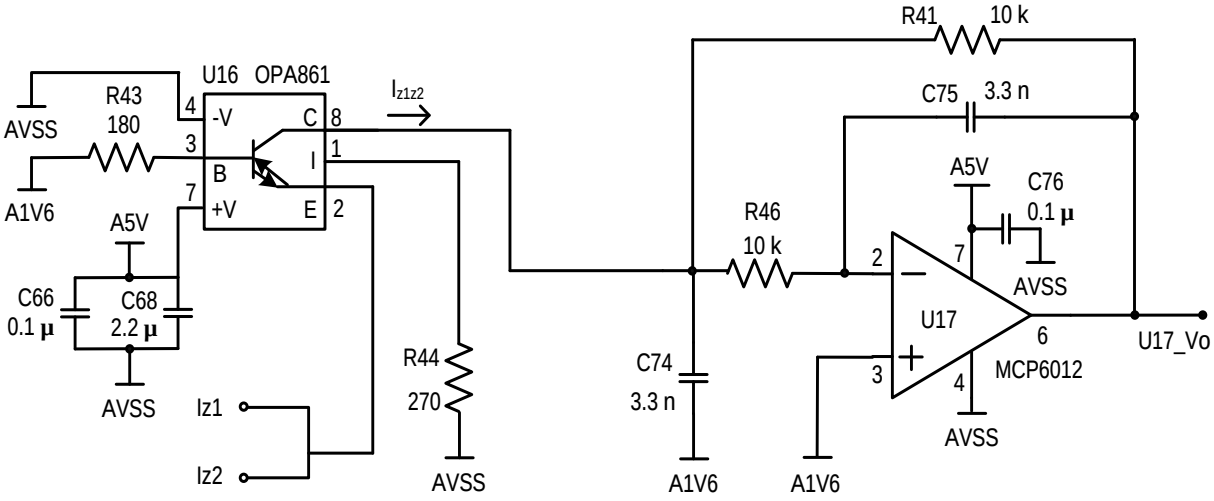

Figure 4.13: Circuit of current summer and low pass filter.

$$\frac{V_{o(U30\_Vo)}(s)}{I_{z1z2}(s)} = \frac{-R_{41}}{1+sC_{75}(R_{41}+R_{46})+s^2C_{74}C_{75}R_{41}R_{46}} \tag{4.11}$$

For a second order current-to-voltage Butterworth low-pass filter with cut-off frequency ω_c, we have,

$$\frac{V_o(s)}{I_{z1z2}(s)} = \frac{R_t}{1+\sqrt{2}(s/\omega_c)+(s/\omega_c)^2} \tag{4.12}$$

Thus, we need to have

$$\frac{R_{41}+R_{46}}{\sqrt{R_{41}R_{46}}}\sqrt{\frac{C_{75}}{C_{74}}} = \sqrt{2} \tag{4.13}$$

$$\omega_c = \frac{1}{\sqrt{R_{41}R_{46}C_{74}C_{75}}} \tag{4.14}$$

To meet the condition in (4.13), we have selected $R_{46} = R_{41}$ and $C_{74} = 2C_{75}$. Thus we get the cut-off frequency ω_c and trans-resistance R_t as the following

$$\omega_c = \frac{1}{\sqrt{2}R_{41}C_{75}} \tag{4.15}$$

$$R_t = -R_{41} \tag{4.16}$$

With R41 = 10 kΩ and C75 = 3.3 nF, we get a cut-off frequency of 3.5 kHz and trans-resistance of 10 kΩ.

The change in output voltage of the circuit for excitation current with peak-to-peak value of I_{pp} and ΔR the change in the resistance being measured is given by,

$$\Delta V_o = \frac{(2I_{pp}/\pi)\cdot\Delta R\cdot A_v\cdot R_{41}}{R_{35}+(2/g_m)} \tag{4.17}$$

where, Av is the gain of instrumentation amplifier, and R35 is the resistance connected across the emitter terminals of U24 and U26. With Av = 10, 1/gm = 10.5 Ω, and R35 = 270 Ω, we have

$$\Delta V_o = 219 I_{pp}\Delta R \tag{4.18}$$

For I_{pp} of 1 mA, the circuit has a sensitivity of 219 mV/Ω.

The low pass filtered output is the impedance variation signal $z(t)$ or impedance glottogram.

4.6 Baseline restoration

Baseline restoration is needed to keep the output signal within the pre-specified upper and lower threshold using a digital potentiometer. The complementary current outputs of U13 and U14 are connected to D3 and D4 of anlog switch U15 as shown in Figure 4.12. The amplitude of input voltage signal to U13 is controlled by the programmable digital potentiometer U6, as shown in Figure 4.3.

The demodulated output *Z(t)* is sampled by on-chip ADC of the microcontroller. It is then compared with the pre-defined threshold limits. If the sampled value crosses the upper threshold limit then amplitude of the restoration signal is increased by updating the control word of digital potentiometer. This brings the demodulator output back to the pre-specified range. And if the output crosses the lower threshold limit then a decrease in amplitude of restoration signal causes the demodulated output to increase and keep it within the range.

4.7 High impedance indicator

A high impedance indicator is used to indicate an inappropriately connected electrode. When the contact between the skin-electrode interface is not proper, demodulator output will get saturated because of the high impedance. The demodulator output is sampled by the on-chip ADC in the microcontroller and compared with the threshold value. If the sampled value is larger than the threshold value, high impedance is indicated by glowing the LED, D6 connected to pin 36 of the microcontroller as shown in the Figure E.5 in the appendix E.

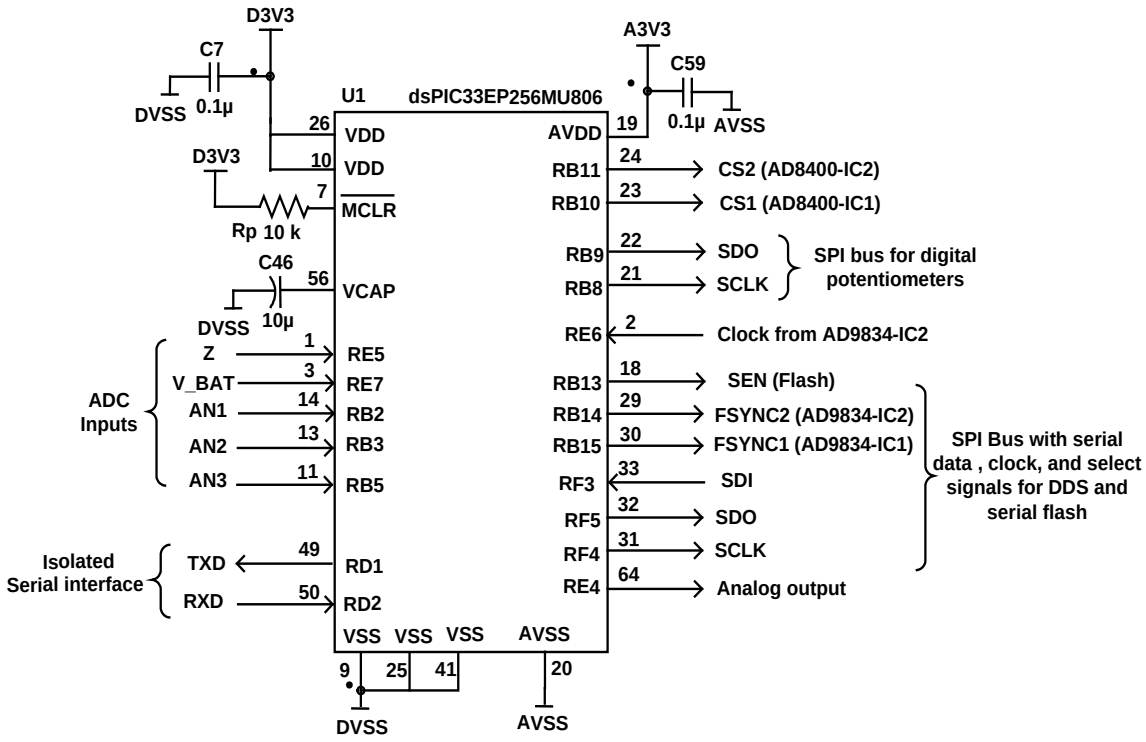

Figure 4.14: Microcontroller circuit.

4.8 Microcontroller

The control and signal acquisition operations in the circuit are handled by a microcontroller. The microcontroller dsPIC33EP256MU806 (Microchip) [47] is used as U1, as shown in Figure 4.15. It can be powered by 3.0–3.6 V separate supplies for analog and digital part. The maximum clock frequency is 80 MHz, resulting in 40 MIPS. Its internal RC oscillator and PLL are used for generating clock, thus eliminating use of external clock or crystal.

It has an in-built SPI module operating at clock frequencies up to 10 MHz. The two DDSs and the flash are programmed through SPI interface. U1 also has an on-chip ADC with 10-bit or 12-bit conversion at a maximum sampling rate of 1.1 Mbps and 500 kbps respectively. ADC has 32 input channels with a support for simultaneous sampling on four channels in 10-bit mode. Five channels of ADC are used: one to sample the demodulator output $z(t)$, three general purpose analog input channels, and one for the battery voltage monitoring. The microcontroller has 14 PWM DAC outputs each having 16-bit resolution. One PWM DAC output is used to generate the EGG signal or its differential. The on-chip UART module is used to interface the microcontroller with PC or an external device.

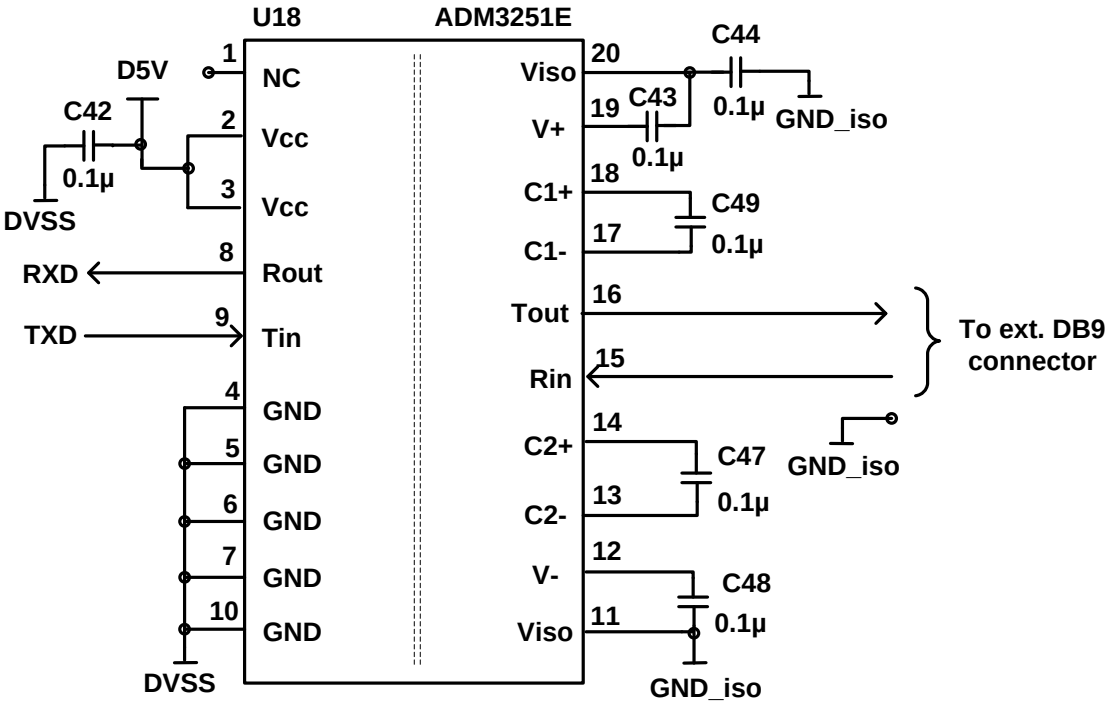

Figure 4.15: Isolated RS232 driver.

4.9 Isolated serial interface

The parameters of the impedance glottograph circuit are set through the serial interface between microcontroller U1 and a PC or an external device. Serial interface is established using an isolated single channel RS-232 line driver ADM3251E (Analog Devices) used as U4. It can operate at 3.3 V supply voltage on the primary side (microcontroller side) with internal charge pump enable to power the secondary side (PC side) with total maximum supply current of 140 mA. The total supply current can be reduced to 12 mA, by powering the secondary side of the line driver from an external source as discussed in section 3.4.2. Parameters for measurement are set using a cable with stereo jack connector J2 on the microcontroller side and DB9 connector on the PC side.

4.10 Analog Input

Three general purpose analog input channels are provided in the design. These channels can be used to feed external signals such as speech or other sensor signals. All the channels are buffered before connecting to the microcontroller pins as shown

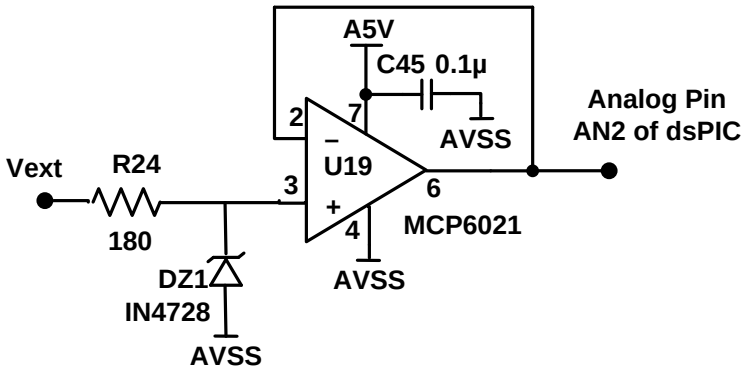

Figure 4.16: Analog input buffer circuit.

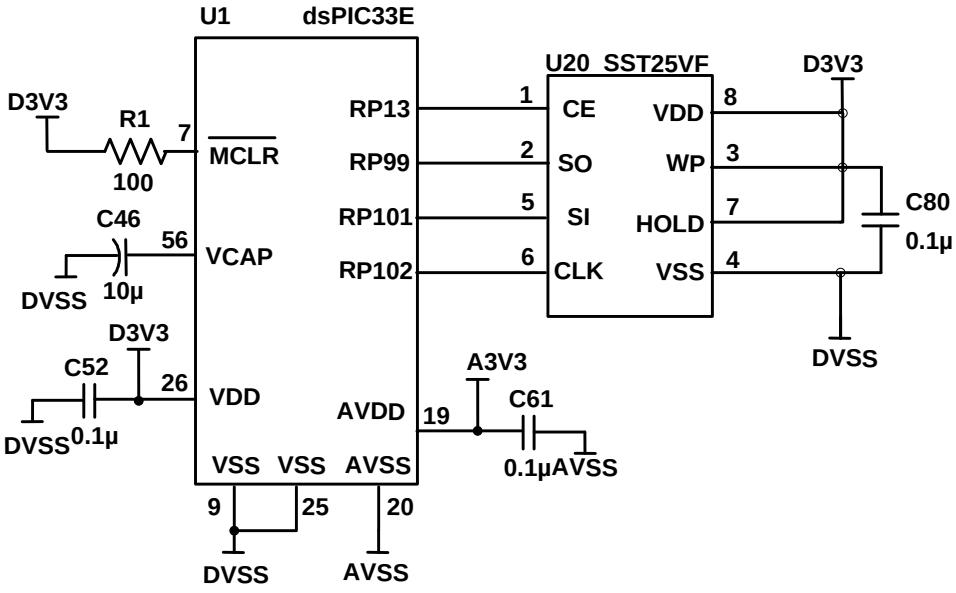

Figure 4.17: circuit of serial flash interface

in Figure 4.16. A 3.3 V zener diode DZ1 is connected at the input of the buffer so that the analog input voltage level does not exceed the ADC input range of 0–3.3 V.

4.11 Flash Memory

An external memory is used to store the EGG samples for further processing. Serial flash IC SST25VF064C (Microchip) [45] used as U19, is interfaced with the microcontroller via SPI interface as shown in Figure 4.16. It has storage capacity of 8 MB and can support up to 80 MHz clock rate for high speed reading. It can operate in the supply range of 2.7–3.6 V supply, with maximum supply current of 20 mA.

4.12 Power Supply

The circuit requires separate analog and digital power supplies. The power supply circuit is shown in Figure 4.18. The total current consumption of the circuit for the analog and digital supplies are estimated as the following

***D3V3 (digital 3.3 V)*:** 39 mA [U2, U3: 3mA, U1: 20 mA, U4: 1 mA, U20: 12 mA]

***D5V (digital 5 V)*:** 143 mA [U15: 1 mA, U5, U6: 1 mA, U36: 140 mA]

***A3V3 (analog 3.3 V)*:** 15 mA [U1: 5 mA, U2, U3: 10 mA]

***A5V (analog 5 V)*:** 50 mA [U29, U7, U17: 2 mA, U11, U12, U13, U14, U16, U8, U9: 6 mA, U10: 2 mA]

Supply voltages of 5 V and 3.3 V are generated using low drop-out (LDO) regulator ICs MCP1802T-5002 (U24,U26) and MCP1802T-3302 (U27,U28) respectively. Each LDO can deliver up to 300 mA load current at 25 µA quiescent current. For 3.3 V operation, the operating input voltage range is 3.6–10 V and for 5 V operation, it is 5.3–10 V. To keep the dissipation in the 3.3 V regulators low, their inputs are obtained from the corresponding 5 V regulators. Thus U24 has to supply 182 mA (143 mA + 39 mA) and U26 has to supply 65 mA (15 mA + 50 mA). Each has a maximum power dissipation of 250 mW at 300 mA load current.

Analog reference of 1.65 V is generated using the voltage divider circuit using R9, R10 and a buffer U8, to facilitate the bipolar voltage swing around 1.65 V as the on-chip ADC of the microcontroller operates at 3.3 V. Analog 5 V and 3.3 V are labeled as A5V and A3V3 respectively, digital 5 V and 3.3 V as D5V and D3V3 respectively and analog reference of 1.65 V is labeled as A1V6.

The LDOs are powered from a DC-DC converter LM2622 (National Semiconductor) used as U23. It has an input voltage range of 2 – 12 V and can give maximum output voltage of 23 V. It operates at a switching frequency of 600 kHz and has a quiescent current of 2 mA. The DC-DC converter is designed to provide 6 V output. A MOSFET switch AM3837 (U22) is used to select the supply source for DC-DC converter. When powered from USB, the switch is turned on and the DC-DC

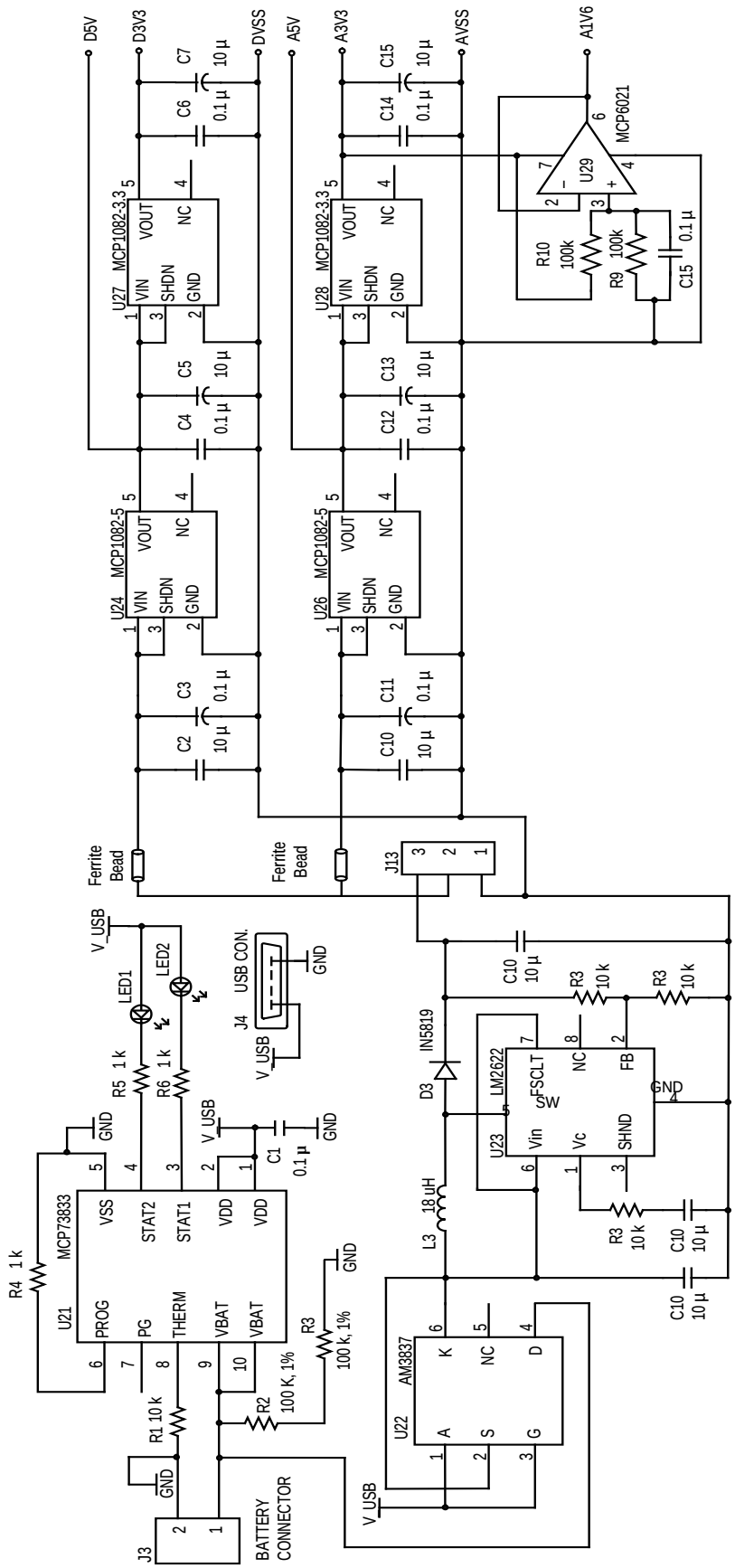

Figure 4.18: Power supply circuit

converter is connected to USB supply. When the USB is disconnected, the switch is turned off and the input is provided from the battery.

A Li-Ion battery with output voltage of 4.2 V when fully charged is used for powering the regulator. Charge capacity of a typical Li-Ion battery is about 1200 mAh. The charger circuit as shown in Figure 3.6, consists of a stand-alone linear Li-Ion charge management controller MCP73833 (Microchip) used as U21. It can operate with supply voltage of 4.5–6 V with maximum supply current of 3 mA. Since temperature sensitivity of U6 is disabled, a 10 kΩ register is connected to THERM as recommended in the datasheet. LED1is used to indicate battery charging and LED2 indicates whether the battery is fully charged.

4.13 Assembly and testing

The component list is provided in Appendix A. The complete schematic of the bioimpedance simulator is given in Appendix B. A double sided PCB was designed for the impedance simulator. Size of the PCB is 89 mm x 152 mm. Components are populated on one side of the PCB. Supply planes are provided on the top layer and ground planes on the bottom layer to reduce the external noise. Care is taken to minimize the length of the supply track for ICs. Supply for each IC is decoupled by 0.1μF capacitors placed as close as possible to the ICs. The component placement with track layout is given in Appendix C. Most of the components used are in SMD packaging. Figures 4.19 and 4.20 shows the images of top and bottom sides of the assembled PCB.

4.14 User interface

User can set parameters such the frequency and amplitude of the excitation current through the user interface provided. It is designed using Visual Basic software. Screenshot of the user interface is shown in Figure 4.21. The PC running the user interface is connected to the microcontroller via serial port. A click on SET button sets the parameters of the microcontroller. Record button is used to record the EGG signal and to store it in the flash. Display button is used to transfer the data from flash to microcontroller.

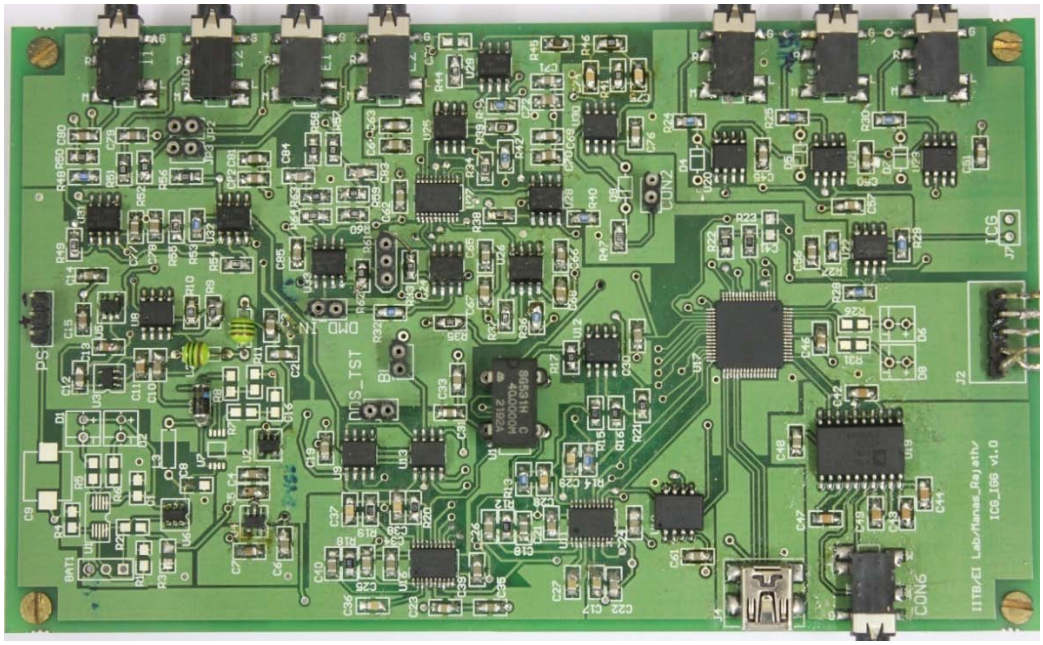

Figure 4.19: Top view of the assembled PCB.

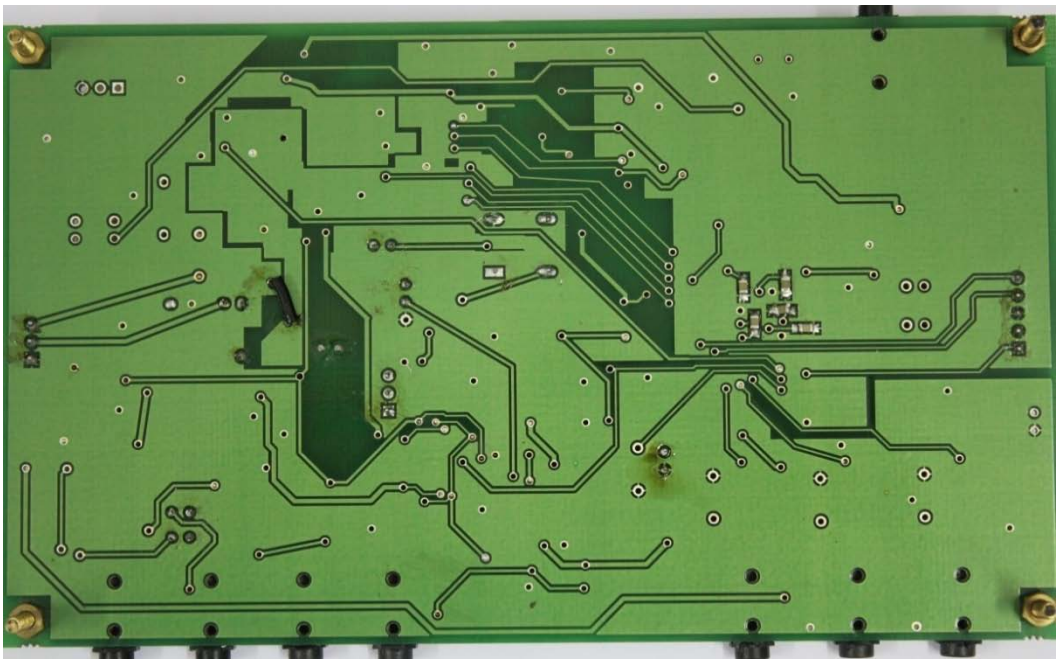

Figure 4.20: Bottom view of the assembled PCB.

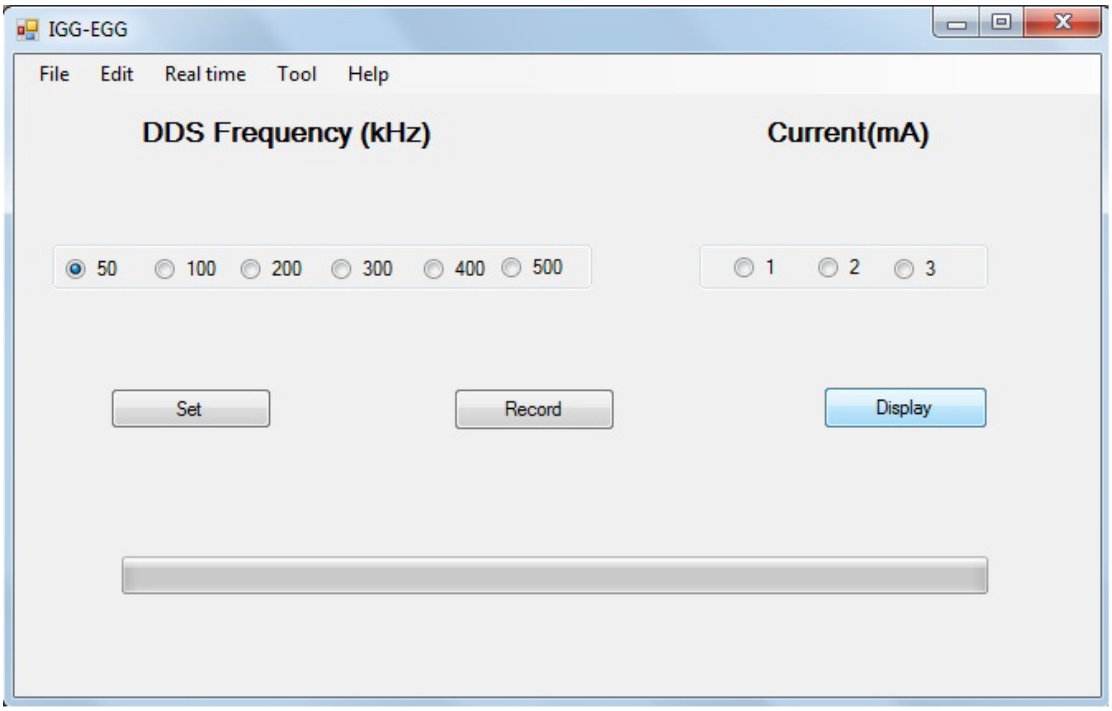

Figure 4.21: Screenshot of the user interface

Chapter 5

TEST RESULT

5.1 Overview

The hardware is tested for linearity, noise rejection, sensitivity, and frequency response using the bio-impedance simulator described in Chapter 3.

5.2 Demodulator output

The filter circuit is disconnected from the demodulator by removing the resistance R45. The capacitor C73, connected to the current summer is replaced by a 100 Ω resistor to observe the full wave rectified signal. An excitation current of 2.5 mA (p-p) with frequency of 100 kHz is injected to a test resistance of 55 Ω. The voltage developed across the injecting electrode is sensed by the voltage-sense-amplifier. It has a gain of 10. The baseline signal for baseline restoration is set at 1.6 V analog reference. The output of the voltage-sense-amplifier along with the baseline signal is fed to analog switch via V-to-I converter circuits. The signal is rectified synchronously with the clock by current steering mode. Figure 5.1 shows the demodulated output along with reference clock captured by the CRO. Phase correction logic is implemented for synchronous demodulation. Phase is corrected until the phase difference between the input signal and the reference clock is minimal. Switching causes spikes in the circuit. The magnitudes of these spikes are small and they cancel out over one cycle of the reference clock. Figure 5.2 shows the demodulator output when the input signal is connected to1.6 V reference signal.

5.3 Linearity

Demodulator module together with lowpass filter is tested for linearity. The output of the demodulator which is passed through the low pass filter is measured for different values of test resistances. The cutoff frequency of low pass filter is set to 5 kHz with unity gain. The amplitude and frequency of the excitation signal is set to 3 mA and 100 kHz respectively. Change in test resistance along with corresponding change the filter output is shown in table 5.1. We can see from the Figure 5.3 that the circuit shows a good linearity over the tested range of test resistances.

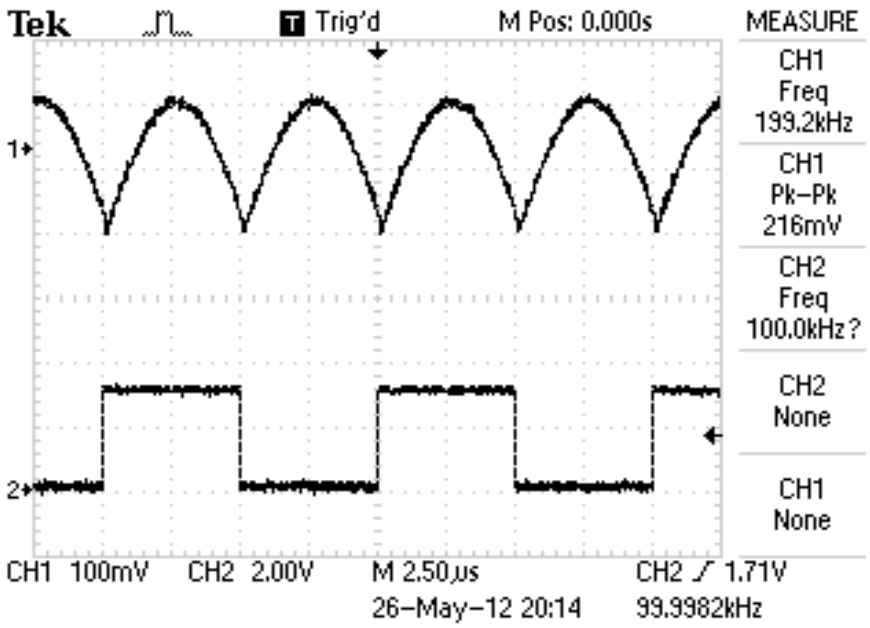

Figure 5.1: Demodulated output (CH1) and reference clock (CH2) with excitation current of 2.5 mA (p-p) and test resistance = 55 Ω.

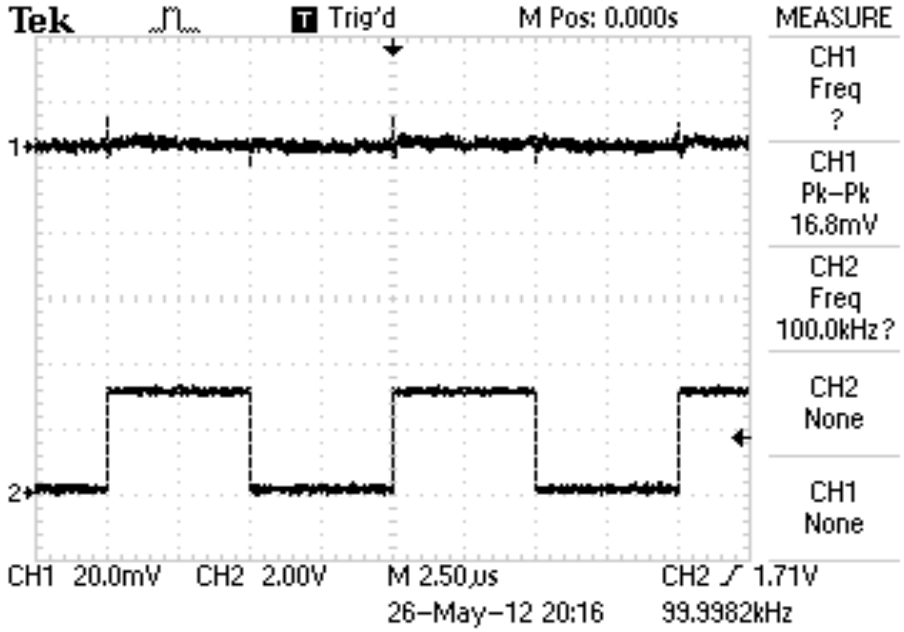

Figure 5.2: Demodulated output (CH1) and reference clock (CH2) with zero excitation current and test resistance = 55 Ω.

Table 5.1 Demodulator output voltages for equal increments in test resistance.

Resistance (Ω)	Demodulator output voltage (V)
10	1.80
20	1.88
30	1.96
50	2.16
60	2.24
70	2.32
100	2.56
110	2.64
120	2.72
130	2.76

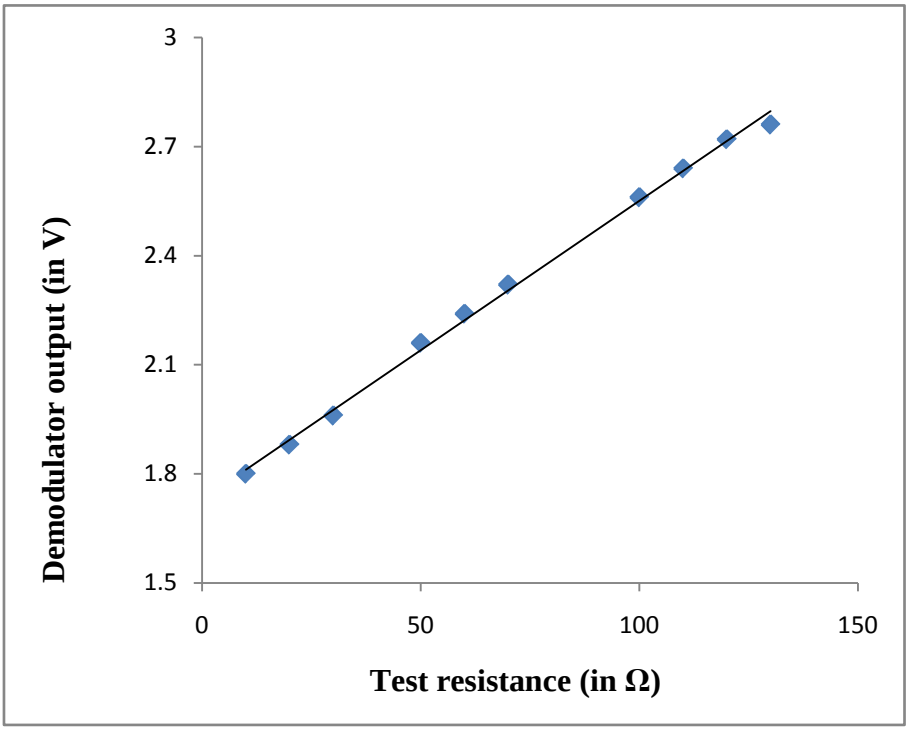

Figure 5.3: Demodulated output voltage Vs test resistances.

5.4 Interference rejection

Interference current at different frequencies are injected in to the test resistance to examine the interference rejection capability of the circuit. A fixed test resistance of

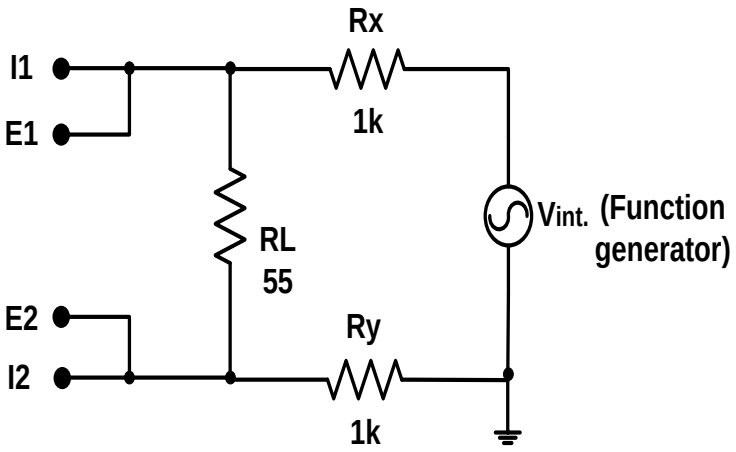

Figure 5.4: Setup for interference rejection testing.

55 Ω is used. The excitation current amplitude was set to zero and frequency was set to 100 kHz respectively. The baseline correction signal was connected to the analog reference of 1.6 V. The interference voltage amplitude was kept at 1 V (p-p) and its frequency was varied from 1 Hz – 1 MHz. Table 5.2 shows the peak-to-peak value of the demodulator output and time period of the of the variations in the demodulator output for different interference frequencies. We can see from the table that interference signal is present mostly at 100 kHz and its odd multiples.

5.5 Validation of hardware using impedance simulator

The bio-impedance simulator discussed earlier was used to test the impedance glottograph. The square wave variation in the resistance provided by the simulator is used to check the sensitivity and frequency response of the hardware. The excitation current amplitude and frequency of the hardware are set to 2.5 mA (p-p) and 100 k Hz respectively. The current injecting and the voltage sensing electrodes of the hardware were connected to the terminals E1 and E2 of the bio-impedance simulator. The voltage is sensed through the voltage-sense-amplifier with gain of 10. The low-pass filter used in the demodulation circuit has a cut-off frequency of 4.8 kHz and a gain of 20. Figure 5.5–5.8 shows the output waveforms for different simulator settings provided in Table 5.3.

Table 5.2: Demodulator output at different interference frequencies

Interference freq. (kHz)	Demod. output ac (mVp-p)	Time period demod. output (ms)
0 – 96	-	-
97	160	0.34
98	160	0.5
98.5	160	0.65
99	190	1
99.2	210	1.26
99.4	220	1.67
99.6	240	2.5
99.8	256	5
100	260	600
100.2	256	4.96
100.4	240	2.49
100.6	224	1.66
100.8	216	1.25
101	196	1
101.5	170	0.67
102	150	0.5
103-297	-	-
298	200	0.5
299	260	1
299.5	328	2
300	370	200
300.5	320	1.98
301	260	1
303 – 498	-	-
499	216	1
500	300	125
502-1000	-	-

Table 5.3: Simulator settings for the outputs shown in Figure 5.5 – 5.8

Figure	R (Ω)	ΔR (Ω)	F (Hz)
5.5	30	0.8	150
5.6	30	0.8	10
5.7	50	0.5	10
5.8	50	1	10

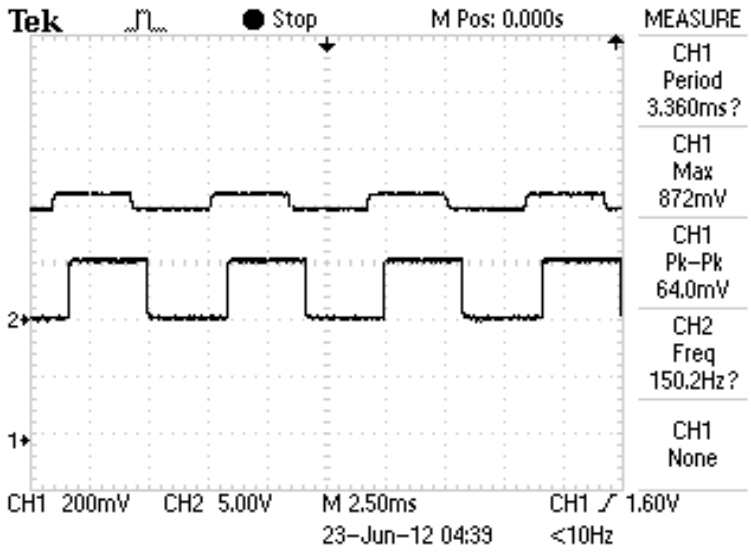

Figure 5.5: CH1: Demod. output for F = 150 Hz, R = 30 Ω and ΔR = 0.8 Ω. CH2 : Clock output from the impedance simulator

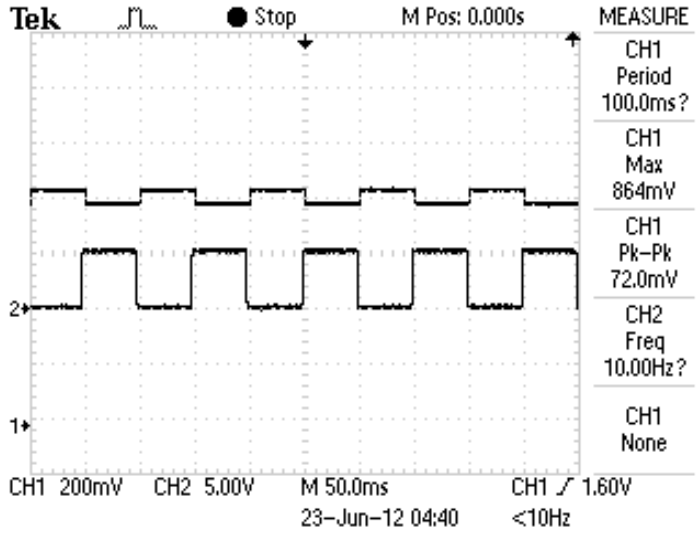

Figure 5.6: CH1: Demod. output for F = 10 Hz, = 30 Ω and ΔR = 0.8 Ω. CH2: Clock output from the impedance simulator

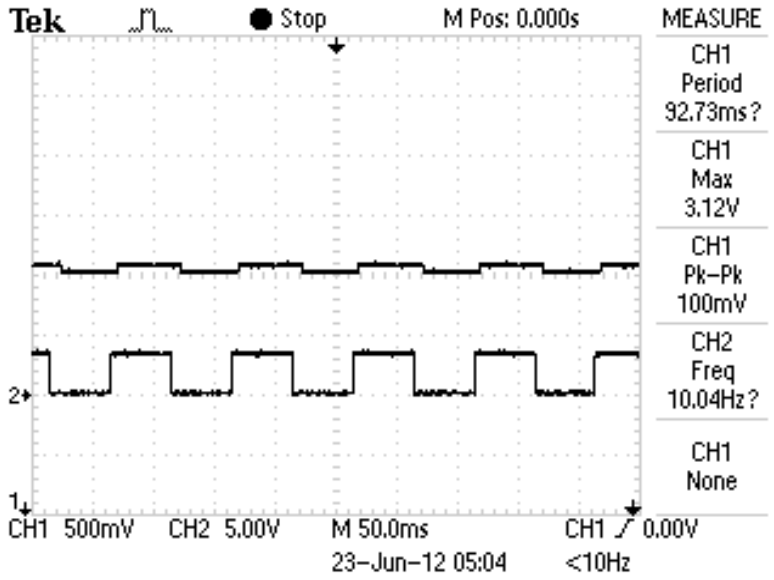

Figure 5.7: CH1: Demod. output for F = 10 Hz, R = 50 Ω and ΔR = 0.5 Ω. CH2 : Test output from the impedance simulator

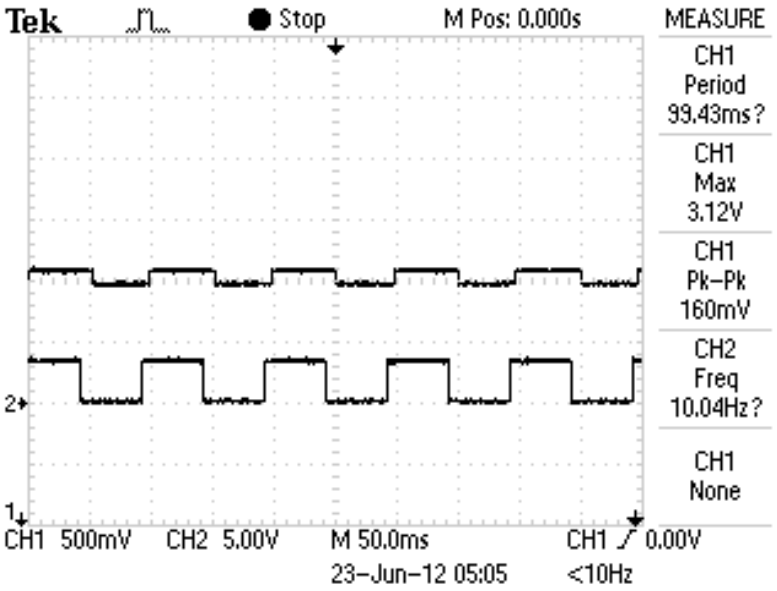

Figure 5.8: CH1: Demod. output for F = 10 Hz, R = 50 Ω and ΔR = 1 Ω. CH2 : Test output from the impedance simulator

Chapter 6

SUMMARY AND CONCLUSIONS

The objective of the project was to develop (a) a laryngeal impedance simulator for testing the sensitivity and frequency response of the impedance glottograph instrument and (b) an impedance glottograph instrument using novel circuits for improving the frequency response and noise rejection.

A laryngeal impedance simulator, using a microcontroller, analog switches, and digital potentiometer is developed. Simulation parameters (frequency, basal resistance and change in basal resistance) are set via PC or an external device through serial port. The device is battery operated and it can provide square wave variation of resistance in the frequency range of 0.1–1 kHz with basal resistance in the range of 10–160 Ω. The simulator has been tested for satisfactory operation.

The impedance glottograph instrument, consisting of a sinusoidal source, voltage-to-current converter, voltage sense amplifier and demodulator has been improvised and tested. Impedance is sensed by generating an excitation signal in the frequency range of 50–500 kHz using a direct digital synthesizer (DDS). This signal is provided to a voltage-to-current converter based on complementary current output configuration designed using a pair of trans-conductance amplifiers to output a low amplitude (< 5 mA) current, which is injected using a pair of electrodes held in contact with the skin on both sides of the thyroid cartilage. The resulting amplitude modulated signal is amplified using a voltage sense amplifier and given to the demodulator. Synchronous demodulation with current steering and baseline restoration circuit is implemented to get the demodulated waveform. Sampling of the demodulator waveform in synchronism with the peaks of the excitation waveform is used for improving the ripple rejection.

The hardware was assembled on a two-layer PCB. Different hardware blocks were tested and found to give satisfactory performance. The dynamic response of the circuit, its sensitivity, and baseline restoration was tested using the bio-impedance simulator. The circuit needs to be thoroughly tested before its clinical use.

Appendix A

GLOTTOGRAPHIC TECHNIQUES

Laryngoscopy is an invasive technique involving illumination and simultaneous viewing of vocal folds vibration. In optical fiber based laryngoscopy, fiberscope is inserted into pharynx through nostril and nasal cavity. An optical fiber is used to illuminate the larynx and to transmit the image back to the optical sensor. The inspection of vibrating vocal folds during speech is possible due to the flexible fiberscope. In direct laryngoscopy, after anaesthesia, a rigid tube is inserted inside the pharynx to observe the movement of vocal folds. In the indirect laryngoscopy, a mirror inserted into back of mouth to view the larynx and vibration of vocal folds. In this technique field of view and large distance from the larynx limits the amount of information. In video laryngoscopy, images of the glottis are obtained by a CMOS active pixel sensors placed at the tip of the laryngoscope blade, which transmits the image electronically to a remote screen. Glidescope, McGrath laryngoscope, and Pentax AWS are some of the commercially available laryngoscopes [3], [4].

Videokymography technique is used to monitor the vibrating vocal folds through a special charge coupled device (CCD) video camera. The camera has two modes, in one mode it works as a regular video camera and in high speed mode the camera delivers images from a single scan line of the whole video field at a rate of 7812.5 line images per second. The consecutive line images are presented below each other on a monitor to create a new, videokymography image which shows vibratory pattern of the selected part of the vocal folds. This technique has lower cost than the high speed imaging method. But full image cannot be obtained due to single line along the glottis [5].

Stroboscope technique involves flashing of a light source with frequency slightly above the fundamental frequency of vibration of the vocal folds. Due to the flashing, difference in frequency of vocal folds and light source, a slow motion illusion of folds is created. This allows easy observation of the vocal folds. It limits the detailed analysis of glottal cycle especially in irregularities consecutive images of

different glottal cycle. Furthermore, stroboscopic image is not a real time continuous signal, therefore it cannot be used for simultaneous recording of audio or other glottographic signals [6].

High speed photography is used to acquire continuous visual data in the form of images on single vocal fold oscillation. An endoscope is used with a camera body containing an image sensor and a digital image memory to capture images. The image sensor was scanned at a high rate and the laryngeal images are stored in image memory. Recent developments include the use of tele-endoscope to obtain accurate information of vocal folds oscillation. The tele-endoscope allows simultaneous capturing of audio, video, and even colour images using contemporary equipment. The disadvantage of the technique is its high cost. It is also invasive and uncomfortable to the patient [7].

Photoglottography (PGG) is a semi-invasive technique in which a photoelectric sensor is placed on the neck below the cricoids cartilage. A fiberscope is used to brightly lit the vocal folds. The light emitted through the glottis and the neck tissues is recorded using the photoelectric sensor. PGG records the change in glottal area in real time, but it is unable to give information about the relative motion of lower and upper vocal fold lips and left and right vocal folds which is a common irregularity in vocal folds pathology [8].

Inverse filtering technique is first introduced by Miller (1951). It is based on source-filter theory of speech production. In principle if transfer function of vocal tract is known then by feeding the speech signal through the inverse of the vocal tract filter, the glottal excitation signal can be reconstructed. Estimation of glottal waveform is difficult for noisy speech signals [9].

Ultrasonoglottography is a noninvasive technique based on transmitting continuous-wave ultrasound through the larynx. Two transducers are used to record echoes from both sides of the glottal rim and pulses transmitted through the larynx. Air is poor medium for ultrasound transmission. When an ultrasound beam of frequency 3.2 MHz is projected across the larynx through transmitting transducer, it is interrupted by the air in the open glottis. When the vocal folds are in contact the wave

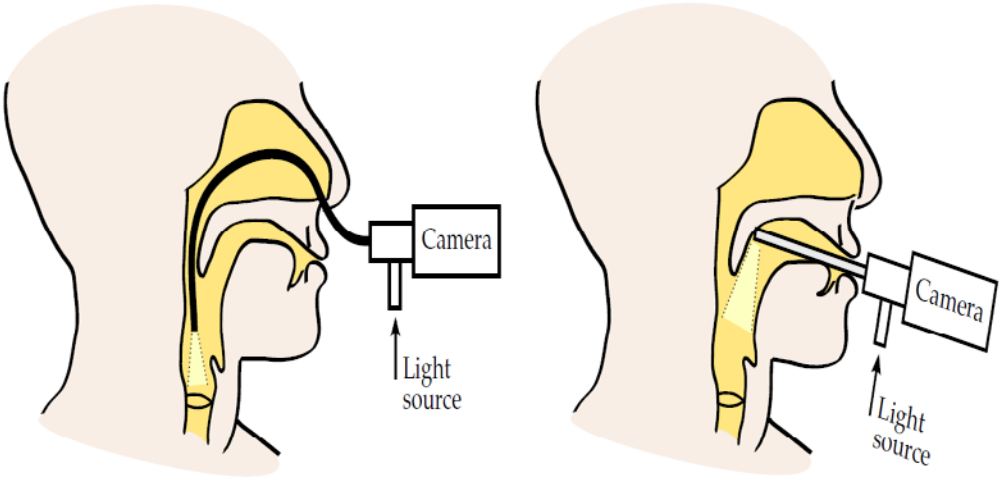

Figure 1.1: A schematic illustration of a fiberscope (on the left) and a solid endoscope for high speed photography (on the right) [13].

is partly transmitted. Thus a change in the vocal folds contact area results in amplitude modulation of the received signal. This technique is safe and comfortable for the subject, but received signals are not uniquely related to the pattern of motion of the vocal folds [10]. Figure 1.1 shows a schematic illustration of a fiberscope (on the left) and a solid endoscope for high speed photography (on the right) [13].

Appendix B

COMPONENT LIST

Table B.1: Component list of the bioimpedance simulator.

Component designator	Component description	Part Number /value	Quantity
C1	Capacitor, ceramic, chip	1 μF	1
C2, C4, C6, C7, C8, C9, C10, C11, C12, C13, C15, C16, C17, C19, C22	Capacitor, ceramic, chip	0.1 μF	15
C3, C5, C14, C20	Capacitor, ceramic, chip	10 μF	4
C21	Capacitor, ceramic, chip	0.01 μF	1
R1, R11, R15, R16	Resistor	10 kΩ	4
R4, R5, R6	Resistor	1 kΩ	3
R13, R14	Resistor	5 kΩ	2
R7	Resistor	10 Ω	1
R8	Resistor	50 Ω	1
R9	Resistor	20 Ω	1
R10, R12	Resistor	100 Ω	2
U1	IC, Charge controller	MCP73833	1
U2	IC, LDO	TC1017–3.3VLT	1
U3	IC, quad analog switch	ADG811	1
U4	IC, digital Potentiometer	AD8400	1
U5	IC, microcontroller	24FJ64GB004	1
U6	IC, RS232 driver	ADM3251E	1
CON1	Connector , 3-pin		1
D1, D2	LED	LED	2
J1, J3	USBCON	USBconMINIB	2
J2	Connector , 5-pin	DEBG	1
J4, J5, J8, J11	Stereo phone jack	PHONEJACK	1
J9	Connector , 2-pin		1

Appendix C

SCHEMATIC DIAGRAM OF THE BIOIMPEDANCE SIMULATOR

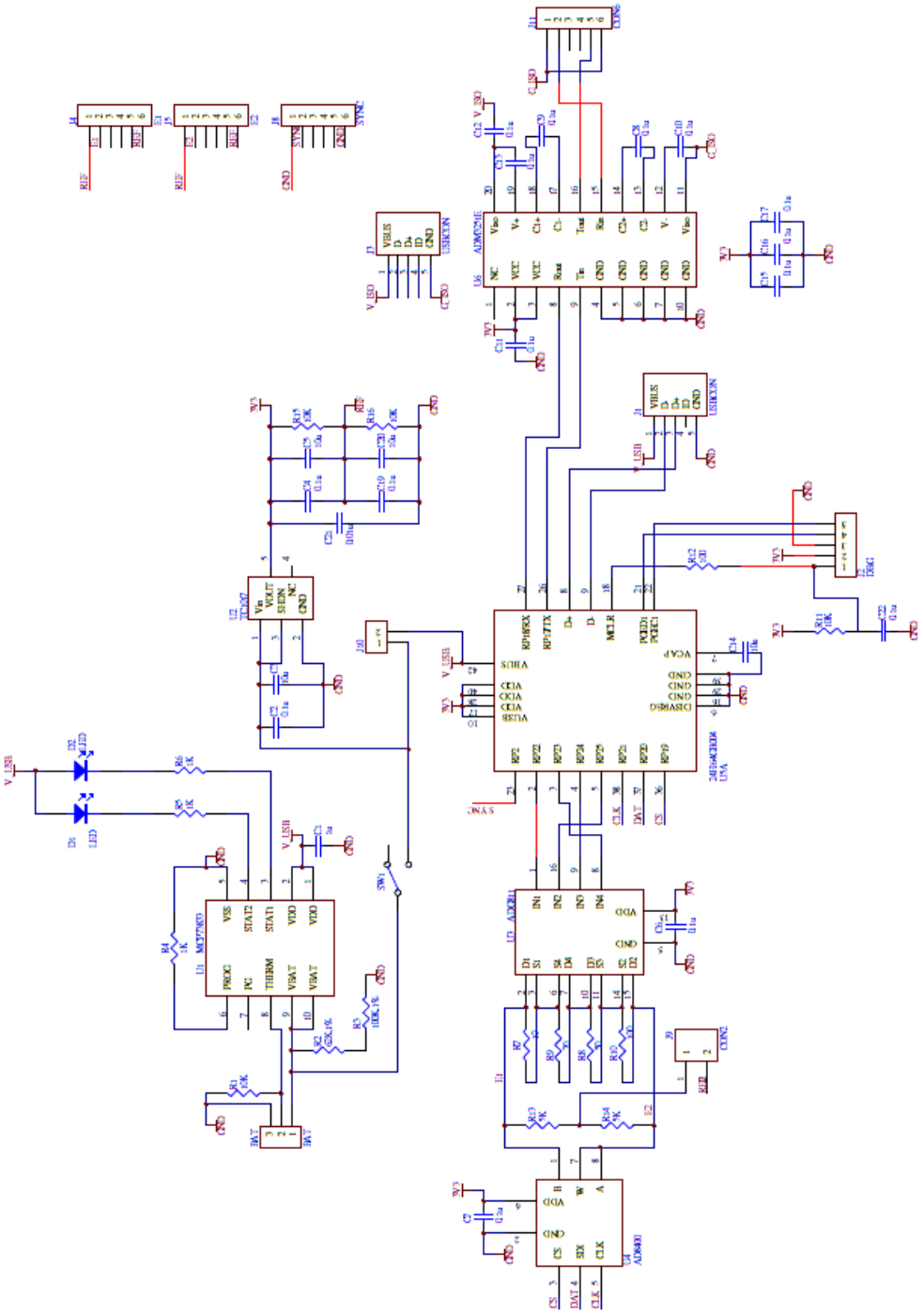

Figure C.1: Schematic diagram of the bioimpedance simulator.

Appendix D

PCB LAYOUT OF THE BIOIMPEDANCE SIMULATOR

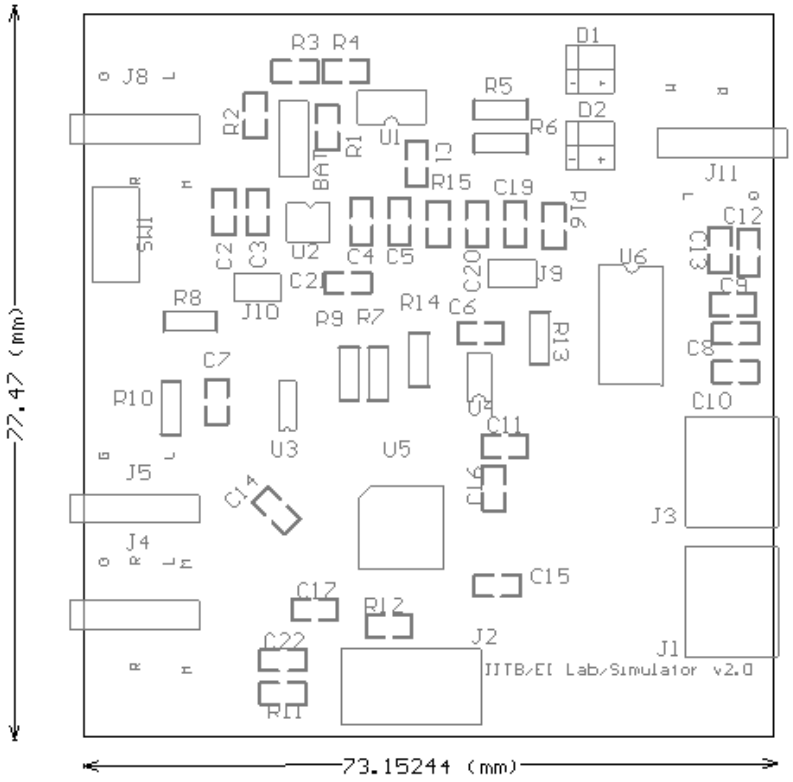

Figure D.1: Top overlay of the bioimpedance simulator (77 mm x 73 mm).

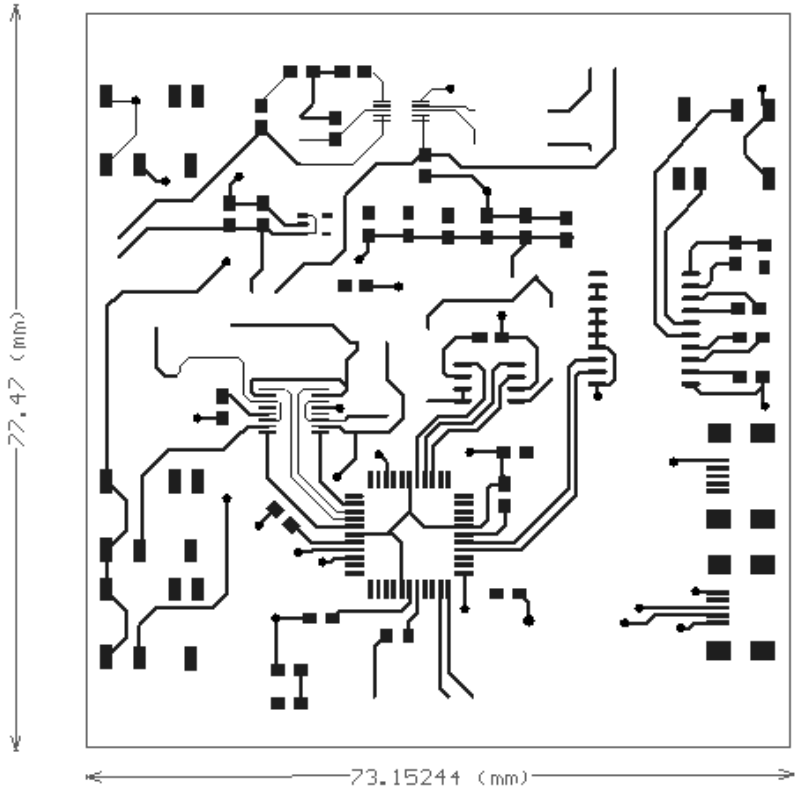

Figure D.2: Top side of the bioimpedance simulator.

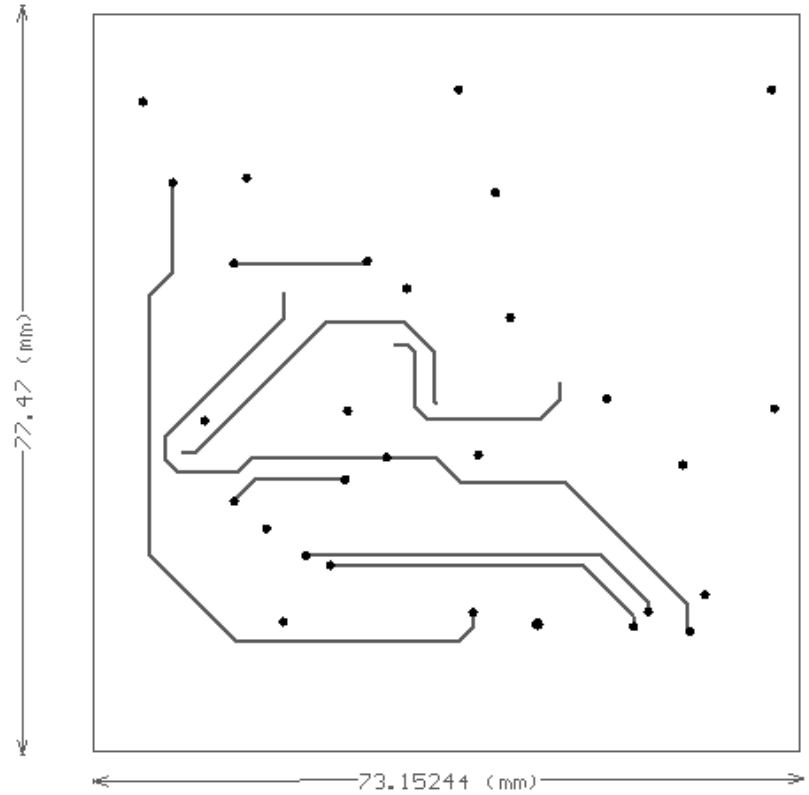

Figure D.3: Bottom side of the bioimpedance simulator.

Appendix E

SCHEMATIC DIAGRAM OF IMPEDANCE CARDIOGRAPH

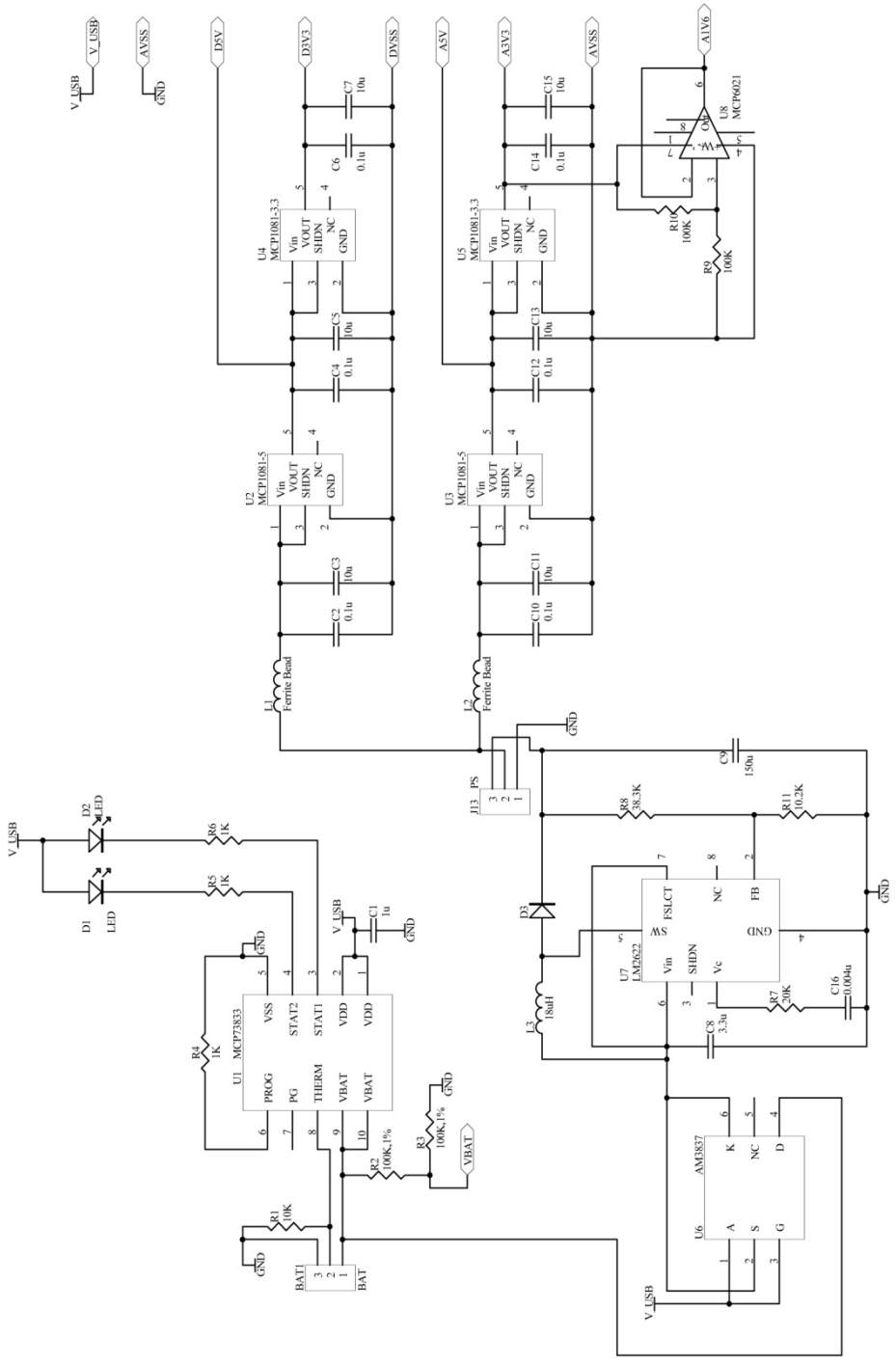

Figure E.1: EGG schematic sheet 1: Power supply.

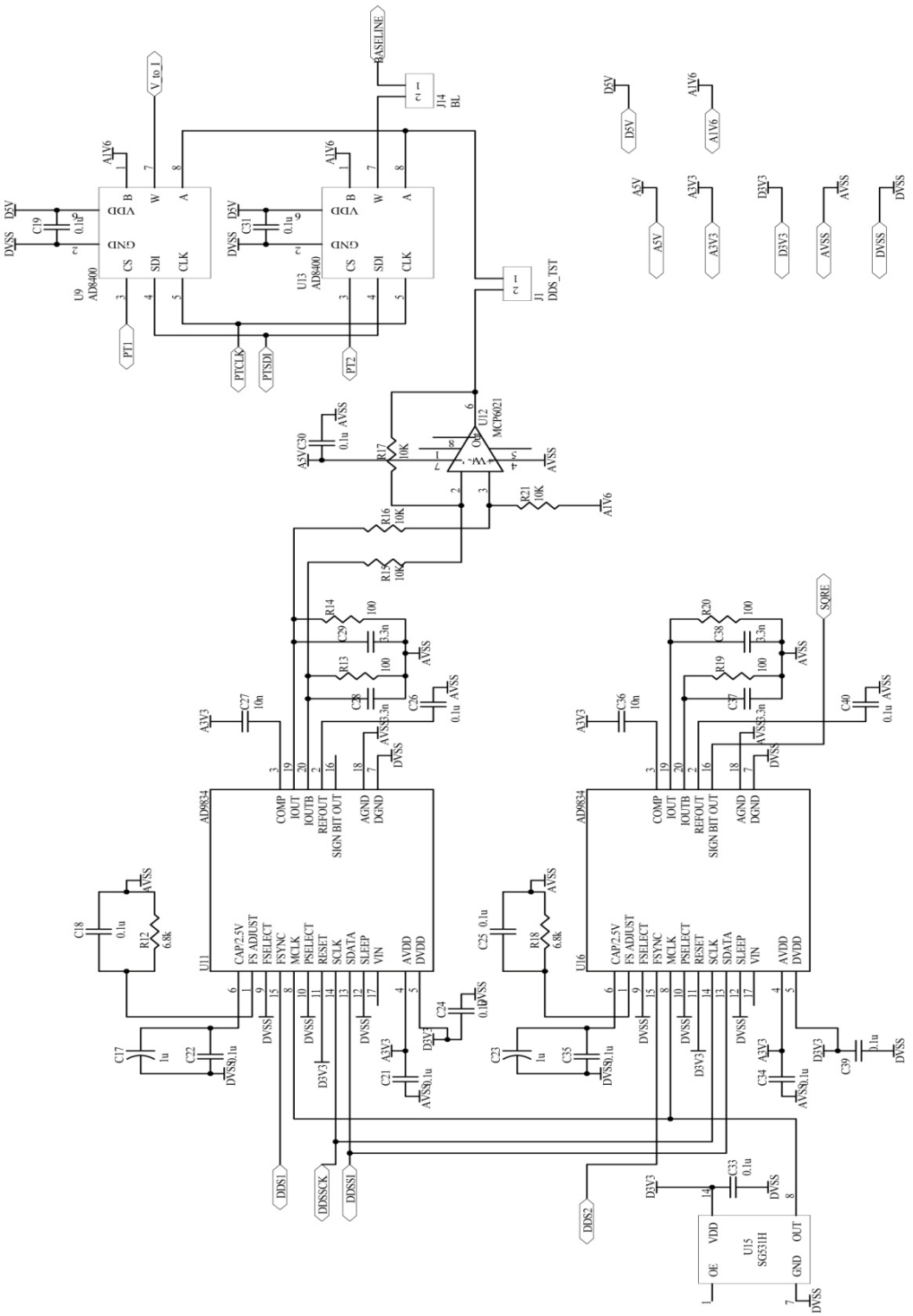

Figure E.2: EGG schematic sheet 2: Waveform generator.

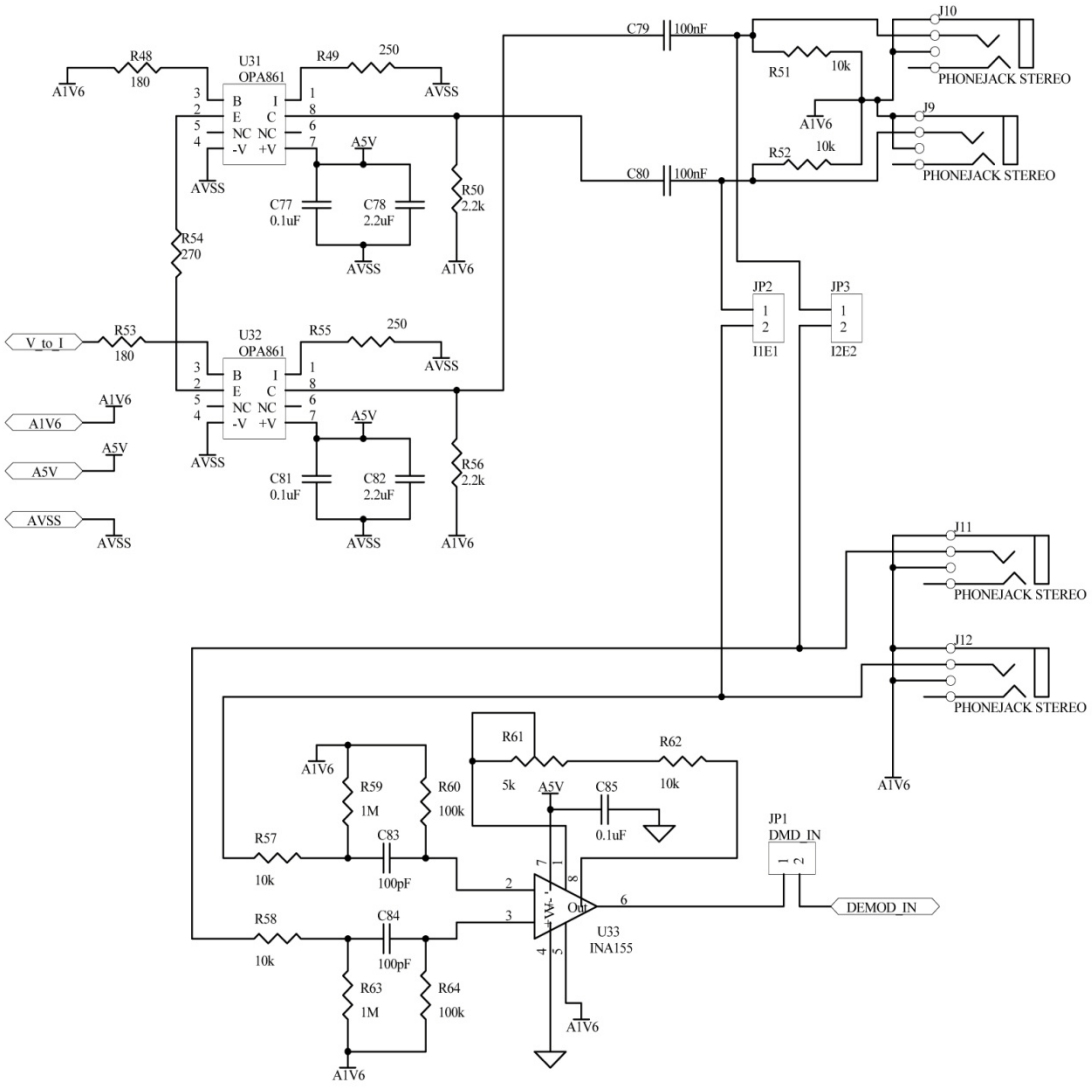

Figure E.3: EGG schematic sheet 3: Current source and ICG amplifier.

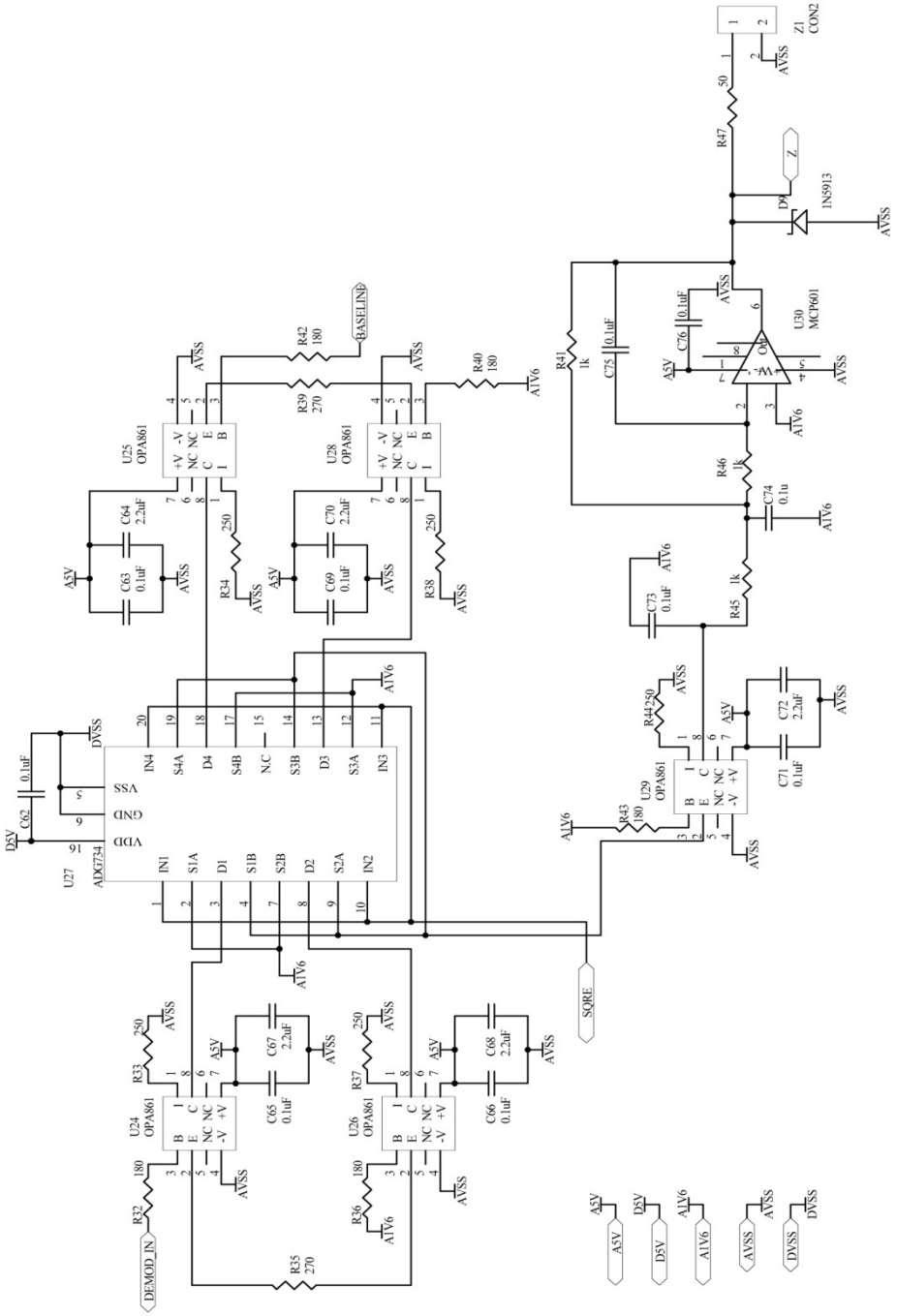

Figure E.4: EGG schematic sheet 4: Demodulator and filter.

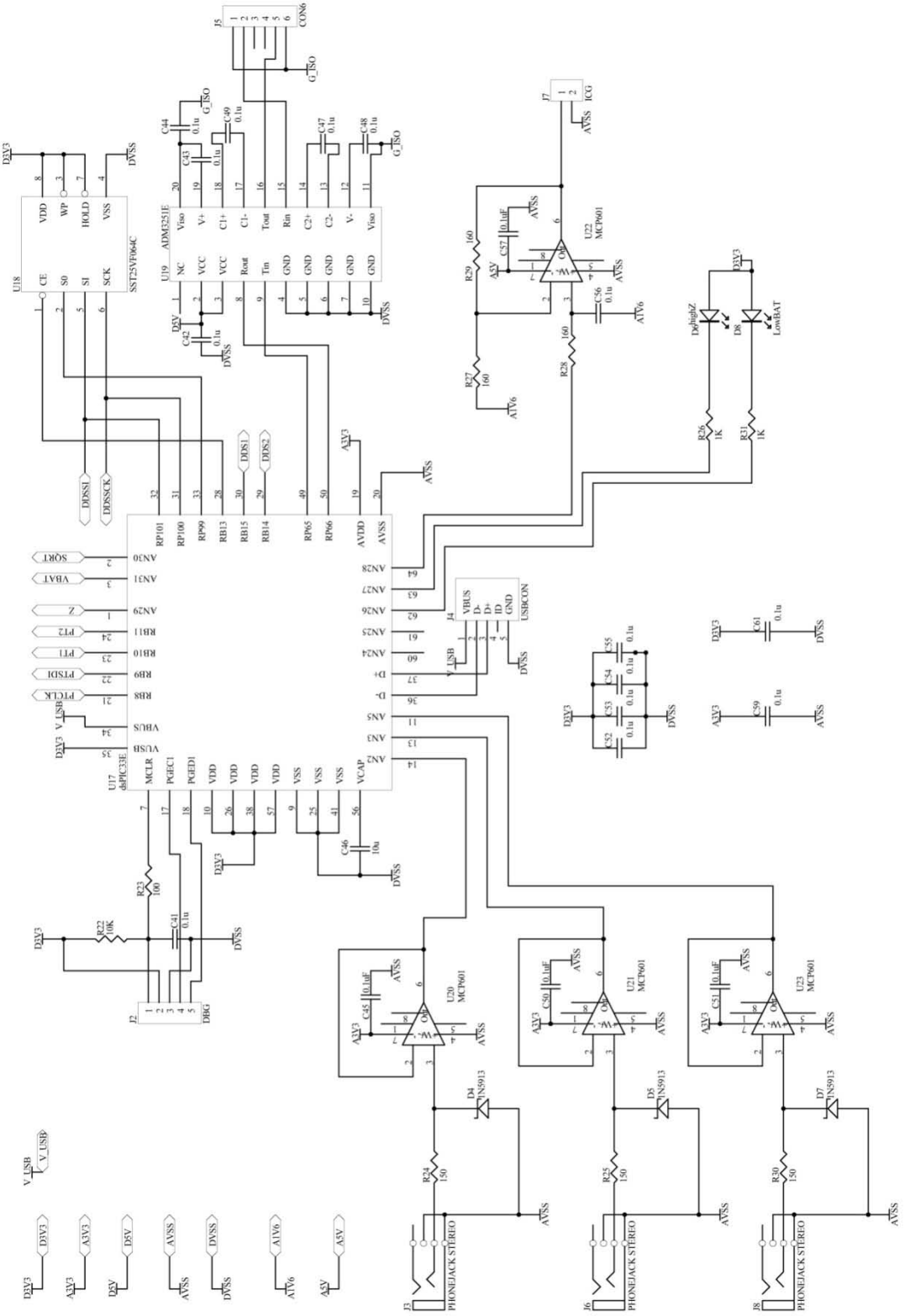

Figure E.5: EGG schematic sheet 5: Microcontroller and serial interface.

Appendix F

PCB LAYOUT OF IMPEDANCE CARDIOGRAPH

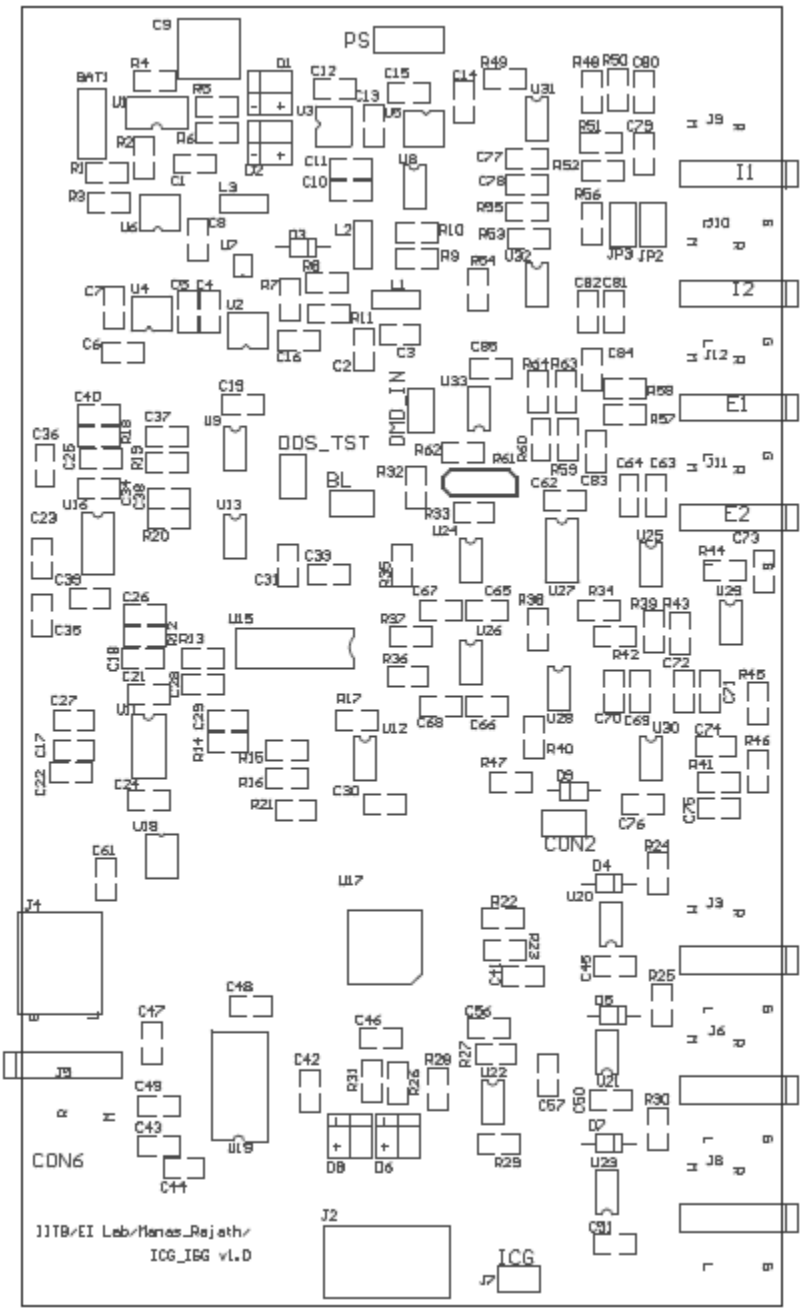

Figure F.1: Top overlay of the assembled PCB.

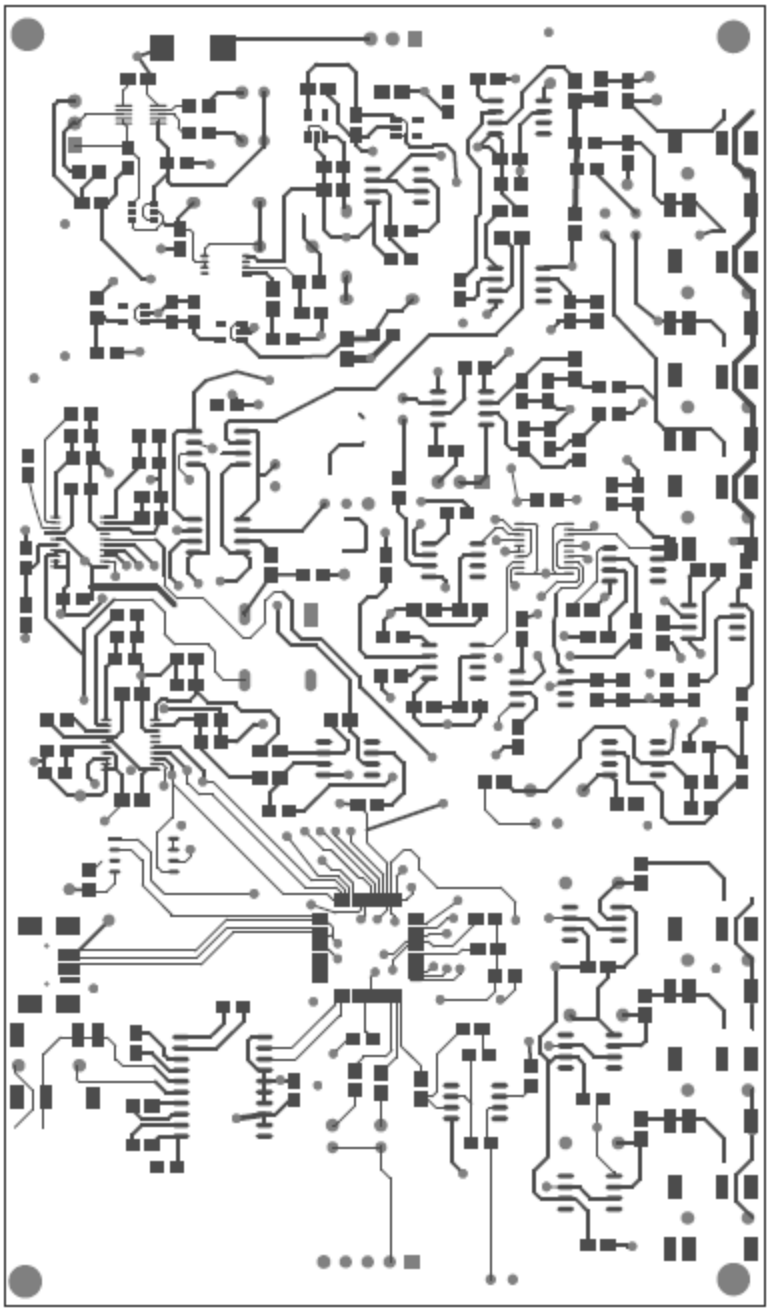

Figure F.2: Top layer of the assembled PCB.

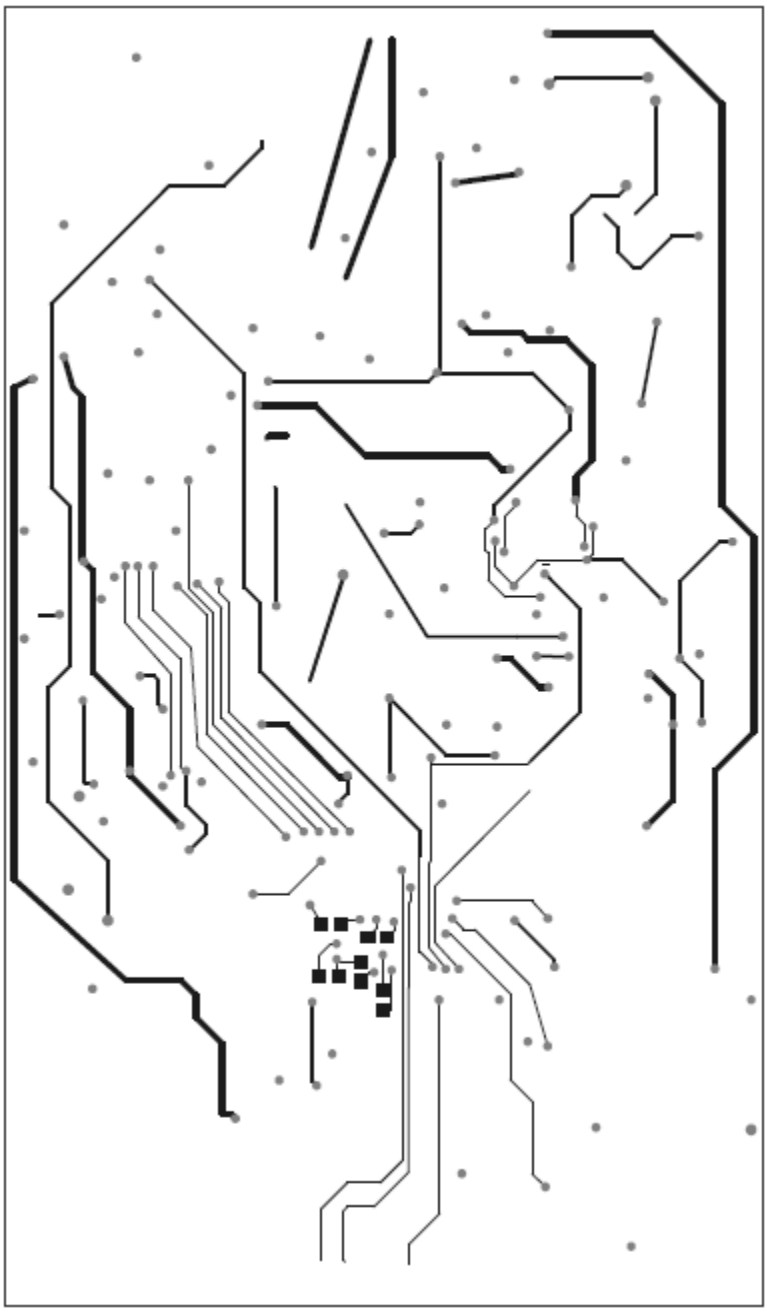

Figure F.3: Bottom layer of the assembled PCB.

REFERENCES

[1] D. O. Shaughnessy, *Speech Communication: Human and Machine,* New York: Addison–Welsey, 1987, pp. 40–47.

[2] A. C. Guyton, *Textbook of Medical Physiology*, Philadelphia, Pennsylvania: Saunders, 4th Ed., 1986, pp. 466–467.

[3] C. Feilding, "The speaking and singing voice," *Tutorial notes*, Auditory Theory: Acoustics, College of Santa Fe Vision, Jan. 2006. Available online, http://www.santafevisions.com/csf/html/lectures/017_instruments_IV.htm, downloaded on 13th October 2011.

[4] K. Marasek, "EGG and voice quality," *Tutorial notes* , Experimental Phonetics Group, Institute of Natural Language Processing, Univ. of Stuttgart, Germany, 1997. Available online, http://www.ims.uni-stuttgart.de/phonetik/EGG/frmst2.htm, downloaded on 20th June 2012.

[5] J. G. Svec, F. Sram, and H. K. Schutte, "Videokymography in 2000: the present state and perspectives of the high-speed line-imaging technique," in *Proc. 4th Int. Workshop on Advances in Quantitative Laryngoscopy, Voice and Speech Research*, 2000, Jena, Thuringia, Germany, pp. 57–62.

[6] eMedicine, "Otolaryngologic and Dental Procedures," available online, http:// emedicine.medscape.com/article/866178-overview, downloaded on 20th June 2012.

[7] S. Kiritani, H. Hirose, and H. Imagawa, "High-speed digital image analysis of vocal cord vibration in diplophonia," *Speech Commun.*, vol. 13, pp. 23–32, May 1993.

[8] C. R. Krausert, A. E. Olszewski, L. N. Taylor, J. S. McMurray, S. H. Dailey, and J. J. Jiang, "Mucosal wave measurement and visualization techniques," *J. Voice*, pp. 1–11, Feb. 2010.

[9] P. Alku, E. Vilkman, and A. M. Laukkanen, “Estimation of amplitude features of the glottal flow by inverse filtering speech pressure signal,” *Speech Commun.*, vol. 24, pp. 123–132, Nov. 1998.

[10] S. L. Hamlet and J. M. Reid, “Transmission of ultrasound through the larynx as a means of determining vocal fold activity,” *IEEE Trans. Biomedical Engineering*, vol. BME-19, no. 1, Jan. 1972.

[11] R. E. Kania, M. Hartl, S. Hans, S. Maeda, J. Vaissiere, and D. F. Brasnu, “Fundamental frequency histograms measured by electroglottography during speech: a pilot study for standardization,” *J. Voice*, vol. 20, no. 1, pp. 18–24, Mar. 2006.

[12] P. K. Lehana and P. C. Pandey, “A low cost impedance glottograph and glottal pitch analyzer,” in *Proc. Int. Conf. on Biomedical Engineering (Bio Vision 2001)*, Dec. 2001, Bangalore, India, pp.33–37.

[13] M. Rothenberg, “A multichannel electroglottograph,” *J. Voice*, vol. 6, no. 1, pp. 36–43, 1992.

[14] K. Than, “In search of music’s biological roots,” *Duke Magazine*, vol. 94, no. 3, pp. 1–3, June 2008.

[15] M. J. V. Garcia, I. Cobeta, G. Martın, H. A. Navarro, and F. J. J. Jimenez “Acoustic analysis of voice in Huntington’s disease patients,” *J. Voice*, pp. 1–10, Aug. 2009.

[16] Speech Lab, “Lx signal,” available online, http://www.reading.ac.uk/ AcaDepts/ll/ speechlab/multichannel/lx/, downloaded on 20th June 2012

[17] J. C. M. Sapienza, E. T. Stathopoulos, and C. Dromey, “Approximation of open quotient and speed quotient from glottal airflow and EGG waveform: effect of measurement,” *J. Voice*, vol. 12, no. 1, pp. 31–43, Feb. 1997.

[18] K. Marasek, “EGG and voice quality,” *tutorial notes* , Experimental Phonetics Group, Institute of Natural Language Processing, Univ. of Stuttgart, Germany, 1997. Available online, http://www.ims.uni-stuttgart.de/phonetik/EGG.htm, downloaded on 20th June 2012.

[19] D. G. Childers and J. N. Larar, “Electroglottography for laryngeal function assessment and speech analysis,” *IEEE Trans. Biomedical Engineering*, vol. BME-31, no. 12, pp. 807–817, Dec. 1984.

[20] Laryngograph Ltd, “Laryngograph processors,” available online, http:// www.laryngograph.com/pdfdocs/speech_studio_usb_with_picture.pdf, downloaded on 20th June 2012.

[21] Vocevista, “VoceVista,” available online, http://www.vocevista.com/, downloaded on 20th June 2012.

[22] WEVOSYS, “lingWaves,” available online, http://www.wevosys.com/products/ lingwaves/lingwaves_electroglottography.html, downloaded on 20th June 2012.

[23] F-J Electronics, “Portable electroglottograph,” available online, http://www. fjelectronics.dk/htm/electroglotto.htm, downloaded on 20th June 2012.

[24] Tiger DRS Inc, “Electroglottograph,” available online, http://www.drspeech. com/ Electroglottograph.html, downloaded on 20th June 2012.

[25] R. Bhagwat / P. C. Pandey (Supervisor), “Glottal pitch extractor,” *B.Tech. Project Report*, Dept. of Electrical Engineering, IIT Bombay, 1990.

[26] M. Chitnis / P. C. Pandey (Supervisor), “A glottal pitch extractor,” *M.Tech dissertation*, Dept. of Electrical Engineering, IIT Bombay, June 1998.

[27] A. V. Patil / P. C. Pandey (Supervisor), “A glottal pitch extractor,” *M.Tech. dissertation*, Dept. of Electrical Engineering, IIT Bombay, Jan. 2000.

[28] A. L. Luthra / P. C. Pandey (Supervisor), “Impedance glottography,” *M.Tech dissertation*, Dept. of Electrical Engineering, IIT Bombay, July 2004.

[29] J. N. Sarvaiya / P. C. Pandey (Supervisor), “Development of an impedance glottograph,” *M Tech. dissertation*, Biomedical Engineering Group, School of Biosciences and Bioengineering, IIT Bombay, July 2006.

[30] N. Mandloi / P. C. Pandey (Supervisor), “Development of an impedance glottograph,” *M Tech. dissertation*, Biomedical Engineering Group, School of Biosciences and Bioengineering, IIT Bombay, June 2011.

[31] J. N. Sarvaiya, V. K. Pandey, and P. C. Pandey, “An impedance detector for glottography,” *IETE J. Research*, vol. 55, no. 3, pp. 100–105, 2009.

[32] Microchip Technology, “8-Bit, CMOS Microcontrollers with LCD Driver and nano Watt XLP Technology,” available online, http://ww1.microchip.com /downloads/en/DeviceDoc/41364E.pdf, downloaded on 20th June 2012.

[33] B. M. Oliver, “Square-wave and pulse testing of linear systems,” in B. M. Oliver and J. M. Cage (Eds), *Electronic Measurements and Instrumentation*, McGraw Hill, Singapore 1975.

[34] M. Desai / P. C. Pandey (Supervisor), “Development of an impedance cardiograph,” *M.Tech. dissertation,* Biomedical Engineering Group, Department of Biosciences and Bioengineering, IIT Bombay, June 2012.

[35] M. Rothenberg, “Tracking multielectrodeelectroglottograph”, U.S. Patent 4,909,261, Mar. 20, 1990.

[36] A. J. Fourcin, “*Laryngographic examination of vocal fold vibration*”, in B. Waye (ed.), Ventilatory and Phonatory Control System. Oxford University Press, 1974.

[37] V. K. Pandey, P. C. Pandey, and J. N. Sarvaiya, “Impedance simulator for testing of instruments for bioimpedance sensing,” *IETE J. Research*, vol. 54(3), pp. 203 - 207, 2008.

[38] Microchip Technology, “PIC24FJ64GB004 Family Data sheet,” available online, http://ww1.microchip.com/downloads/en/DeviceDoc/39940d.pdf, downloaded on 20th June 2012.

[39] Analog Devices, "20 mW power, 2.3 V to 5.5 V, 75 MHz complete DDS AD9834," Available online, www.analog.com/static/importedfiles/ Data_Sheets/AD9834.pdf, downloaded on 20th June 2012.

[40] Analog Devices, “Digital Potentiometer," Available online, www.analog.com/static/importedfiles/Data_Sheets/AD8400.pdf, downloaded on 20th June 2012.

[41] Microchip, "Rail-to-rail input/output, 10 MHz op-amps," Available online, ww1.microchip.com/downloads/en/DeviceDoc/21685d.pdf, downloaded on 20th June 2012.

[42] L. Venkatachalam / P. C. Pandey (Supervisor), “Development of hardware for impedance cardiography”, M.Tech. Dissertation, Biomedical Engineering Group, School of Biosciences and Bioengineering, Indian Institute of Technology Bombay, 2006.

[43] Texas Instruments, “Wide Bandwidth Trans-conductance Amplifier”. Available online, http://focus.ti.com/lit/ds/symlink/opa861.pdf, downloaded on 20th June 2012.

[44] Analog Devices, “CMOS, 2.5 Low Voltage, Triple/Quad SPDT Switches”. Available online, http://www.analog.com/static/imported-files/data_sheets/ ADG7 33_734.pdf, downloaded on 20th June 2012.

[45] Microchip, "64 Mbit SPI Serial Dual I/O Flash," Available online, ww1 http://ww1.microchip.com/downloads/en/DeviceDoc/25036A.pdf, downloaded on 20th June 2012.

[46] Analog Devices, "Isolated, single-channel, RS232 line driver/receiver," Available online, www.analog.com/static/importedfiles/Data_Sheets/ ADM3215E.pdf, downloaded on 20th June 2012.

[47] Microchip, "High performance 16-bit digital signal controllers," Available online, http://ww1.microchip.com/downloads/en/DeviceDoc/70616F.pdf, downloaded on 20th June 2012.

Acknowledgements

I express my sincere gratitude towards Prof. P. C. Pandey for the guidance and support he gave me during this project. He introduced me to the world of speech processing and bio-medical instrumentation, encouraged me to take up new challenges and inspired me all throughout my stay here.

I am thankful to Nandakumar Pai for his valuable time and support he gave for this project. I would like to thank Vidyadhar Kamble for helping me in all the lab related issues. I am greatly indebted to Nataraj and Jagbandhu for making my stay here more memorable. I am also thankful to all my friends especially in the SPI Lab, EI Lab for their whole-hearted support during the tenure of this project.

Finally, I would like to thank Manaskant Desai for the great time I had working with him for this project.

P. S. Rajath Bhat

Author's resume

P. S. Rajath Bhat: He received the B. E. Degree in electronics and communication engineering from B. T. L. Institute of Technology, Bangalore, Karnataka in 2007. He worked as Project Associate at Analog Devices Inc Lab, IIT Madras from May 2008 to June 2009. Presently he is pursuing the Master of Technology degree in electrical engineering at the Indian Institute of Technology Bombay. His research interests include digital signal processing, speech processing and embedded system design.

Publication

A. R. Jayan, P. S. Rajath Bhat, and P. C. Pandey, "Detection of burst onset landmarks in speech using rate of change of spectral moments," *Proc. National Conference on Communications 2011* (NCC 2011), Bangalore, India, paper SpPrI.3.